Hydrogen Storage Properties of Mg-Ni-H through Pressure Composition Isotherms Combined with Thermodynamic Calculations

Guy-Joël Rocher

A Thesis

in

The Department

of

Mechanical and Industrial Engineering

Presented in Partial Fulfillment of the Requirements

For the Degree of Master of Applied Science (Mechanical Engineering) at

Concordia University

Montréal, Québec, Canada

December, 2012

CONCORDIA UNIVERSITY
School of Graduate Studies

This is to certify that the thesis prepared

By: Guy-Joël Rocher

Entitled: *Hydrogen Storage Properties of Mg-Ni-H through Pressure Composition Isotherms Combined with Thermodynamic Calculations*

and submitted in partial fulfillment of the requirements for the degree of

Master of Applied Science (Mechanical Engineering)

complies with the regulations of the University and meets the accepted standards with respect to originality and quality.

Signed by the final examining committee:

_____ Chair
Dr. I. Contreras

_____ External Examiner
Dr. G. Gopakumar

_____ MIE Examiner
Dr. M. Pugh

_____ Supervisor
Dr. M. Medraj

_____ Supervisor
Dr. H.D. Ng

Approved by _____
Dr. S. Narayanswamy, Graduate Program Director

_____
Dr. Robin A.L. Drew, Dean
Faculty of Engineering & Computer Science

Date December 6, 2012

ABSTRACT

Hydrogen Storage Properties of Mg-Ni-H through Pressure Composition Isotherms combined with Thermodynamic Modeling

Guy-Joël Rocher

Concordia University, 2012

Environmental concerns have fueled the development of alternative sources of energy for many decades. Amongst the list of viable options to petroleum products stands hydrogen. However, a number of technological barriers prevent the wide-spread use of hydrogen energy such as safety and more importantly storage. The primary objective of this work is to investigate experimentally the hydrogen storage properties of metal hydrides with the focus on the Mg-Ni-H system.

Namely two compositions were analyzed in this system $Mg_{66}Ni_{33}$ and $Mg_{72}Ni_{28}$. Pressure composition isotherm (PCI) experiments were carried out using a Sievert's type apparatus and sample characterization was performed using X-Ray diffraction (XRD). The obtained PCI data, XRD patterns and Van't Hoff plots for the $Mg_{66}Ni_{33}$ composition were found to be in good agreement with literature data. In addition, original results were obtained for the $Mg_{72}Ni_{28}$ sample which allowed to observe the catalytic role of Ni in hydride reactions.

Furthermore, the collected experimental results were compared to thermodynamic calculations obtained using the CALPHAD method with Factsage software package. Good agreement was again observed thus supporting the combined thermodynamic

modeling and key experiments methodology which considerably accelerates the study of a metal hydride system when compared to performing only experiments.

ACKNOWLEDGEMENTS

I would like to express my appreciation to my supervisors, Dr. Mamoun Medraj and Dr. Hoi Dick Ng, for their time, suggestions, and continuous support during my MASc project at Concordia University.

I am greatly indebted to Dr. Jacques Huot from Université de Trois-Rivières for granting me access to his facilities at IRH and his students especially Julien Lang and Manuel Toussignant for their assistance. In addition, I am grateful to Mohammad S. Askari and Dr. Xavier Ottenwaelder for granting me access to their glove box. I would like to thank my colleague Saida Abdessameud, PhD candidate for her thermodynamic calculations and research associate, Dr. Dmytro Kenorkov, for his assistance in analyzing experimental data. Many thanks also go to the administrative staff: Sophie Mérineau, Maureen Thuringer and Arlene Zimmerman.

I cannot forget to thank all my group members sharing so many laughs with me and especially Ahmad Omar for his help and support.

Last but not least, much love and gratitude goes out to my family and my better half Carlie for their unwavering love, endless support and devoted encouragement.

Table of Contents

List of figures

List of tables

Chapter 1

Hydrogen Energy: INTRODUCTION

Human activity has been releasing greenhouse gases in the environment for thousands years. However, industrialization advancements over the past two centuries are responsible for far more greenhouse gas emissions than the cumulated amounts from the millenniums that preceded. Though on the political scene, environmental concerns have been identified as important only recently, increases in greenhouse gas emissions have been linked to climate change by experts of governmental agencies as early as the 1960s, as shown in this excerpt from a report by the US National Academy of Sciences presented to President Kennedy.

> *"There is evidence that the greatly increasing use of the fossil fuels, whose material contents after combustion are principally H_2O and CO_2, is seriously contaminating the earth's atmosphere with CO_2. Analyses indicate that the CO_2 content of the atmosphere since 1900 has increased 10 per cent. Since CO_2 absorbs long-wavelength radiation, it is possible that this is already producing a secular climatic change in the direction of higher average temperatures. This could have profound effects both on the weather and on the ecological balances."* [2]

Thus, it is only a matter of time before environmental degradation will force humans and the other inhabitants of Earth to dramatically alter their lifestyle. In order to avoid such setting, renewable sources of energy with low environmental footprint are

required to ensure an adequate quality of life for the generations to come. One environmentally viable candidate to supply energy needs in the future is hydrogen.

In fact, hydrogen not only is a cleaner alternative to petroleum based energy sources, it is also much more efficient [3]. Although hydrogen can be used as a clean source of energy through combustion, it is rather when used as an energy carrier that it holds the most technological benefits. When employed as such and combined to renewable energy sources such as wind, solar, tidal, etc., hydrogen completes an emission free energy cycle. In addition, hydrogen technologies facilitate localized energy production, which in turn contributes to the reduction of energy dependency on foreign countries. Moreover, secluded regions that currently encounter expensive transportation cost for oil derived products can gain even more from local energy production methods. Finally, hydrogen related technologies strengthen the grid by distributing power sources, which also contributes to improving the flexibility, efficiency and reliability of large scale electrical networks [4].

Another area where hydrogen offers considerable advantages is portable electric products. In fact, the energy storage density of any type of hydrogen fuel cell is substantially larger than conventional liquid electrolyte based batteries. Furthermore, hydrogen fuel cells encounter less energy loss during long term storage and maintain higher charge capacity after extended cycling. The combination of these properties enables hydrogen fuel cell technologies to provide increased performance as energy carriers for mobile electric applications. More specifically, in the case of all electric transportation applications, the hydrogen fuel cell vehicle, shown in Figure 1.1, plays a vital role as it currently is the only technology that offers long range capability.

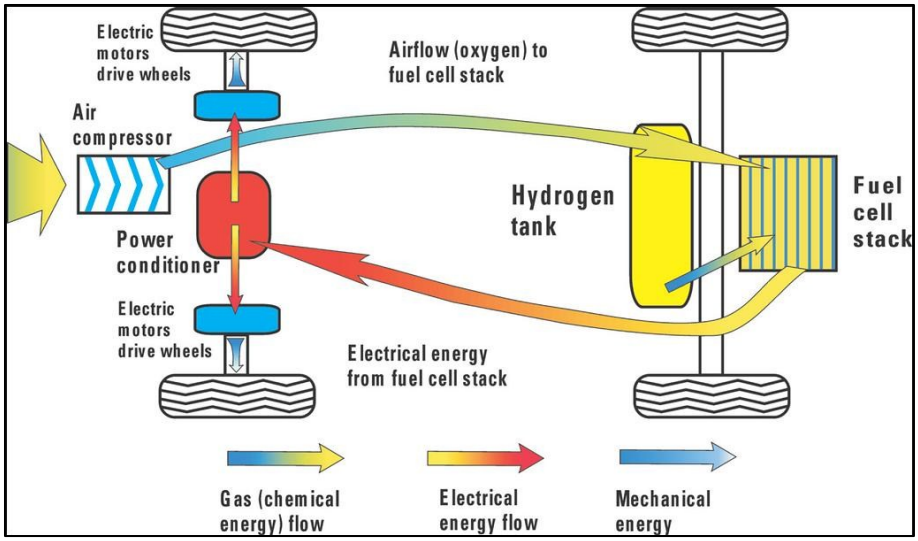

Figure 1.1: Schematic hydrogen fuel cell electric vehicle [5]

While hydrogen offers advantages as an energy carrier, technological barriers impede the introduction of a wide spread hydrogen industry. Numerous technical challenges exist in areas ranging from viable hydrogen production methods all the way down to fuel cell operation. Consequently, various key aspects of this energy carrier require further development to enable extensive use of the technology.

One of these crucial features is safety. Although, hydrogen is the most abundant element in the universe, it is difficult to handle safely when encountered in high purity. It is an invisible, odorless and non-poisonous gas. Due to its low density and high diffusion speed hydrogen spreads quasi-instantly when released in air. The key safety parameters of gasoline, natural gas and hydrogen are shown in Table 1.1. Hydrogen has the widest flammability range of all flammable air mixtures which ranges from 4-75% (Volumetric %), in upwards combustion [6]. This property is often seen as a serious safety hazard since most hydrogen releases in air can propagate a flame. Moreover, it can also be seen in Table 1.1 that the 4.0% lower flammability limit (LFL) of hydrogen is higher than the 1.4% LFL of gasoline vapor, thus hydrogen has a larger flammability safety margin.

Although flame mitigation is of importance, the most critical aspect in the case of catastrophic system failure is the explosion safety margin. Yet again, hydrogen fares better as the lower explosion limit (LEL) of hydrogen is 18.3% and that of gasoline is 1.1%. Therefore, as the critical concentration for flammability and explosion is higher for hydrogen more time is available for shut-down or evacuation procedures.

Table 1.1: Safety Parameters [7]

	Flammability Limits in Air (Volumetric %)	Explosion Limits in Air (Volumetric %)	Stoichiometric Mixture in Air (Volumetric %)	Ignition Energy (MJ)
Gasoline Vapor	1.0 - 7.6	1.1 - 3.3	2	0.2
Natural gas	5.3 - 15	6.3 – 13.5	9	0.29
Hydrogen	4.0 - 75	13 - 65	29	0.02

Besides safety consideration, storage is also an aspect of hydrogen technologies in need of development. In fact, storage remains the critical advancement required to propel the hydrogen segment forward. Due to the extremely low density of hydrogen gas, even under high compression, larger volumes are required to store practical amounts of energy when compared to conventional fuels. In addition, alternative methods that store hydrogen under a different form, such as liquid, also suffer from volume and weight penalties due to the complexity of their storage systems. These limitations hinder the use of hydrogen for non-stationary applications where volume minimization is essential in optimized designs. One key technique that meets gravimetric and volumetric storage requirements is metallic hydride. However, operating temperature and the kinetics of metallic hydrides are outside the operating range of hydrogen fuel cells. Consequently,

storage continues to be the limiting factor for hydrogen technologies for transportation applications.

As a result, in recent years research efforts have turned towards less volume dependent areas such as large scale and remote applications where salt caves storage, underground mining equipment and renewable energy grid level storage offer promising prospective [8]. Nonetheless, the Department of Energy (DOE) of the United States of America established clear and precise performance goals for hydrogen storage in the automobile industry, which have been widely accepted as the performance targets in the research field for most of the past decade.

Therefore, since targets have yet to be quantified for most stationary applications, the transportation field will be the targeted application throughout this work. The light-duty vehicle targets from the DOE are shown in Table 1.2.

Table 1.2: DOE on-board hydrogen storage targets [9]

Storage Parameter	Units	2010	2015	Ultimate
System Gravimetric Capacity Usable specific energy from H_2 (net useful energy / max system mass)	kWh/kg (kg H_2/kg system)	1.5 (0.045)	1.8 (0.055)	2.5 (0.075)
System Volumetric Capacity Usable energy density from H_2 (net useful energy / max system volume)	kWh/m^3 (kg H_2/m^3 system)	0.0009 (28)	0.0013 (40)	0.0023 (70)

Although several methods exist for hydrogen storage, metal hydrides are the most promising as only they offer good reversibility along with good volumetric and gravimetric performance. However, the identification of a metal hydride that meets the DOE targets has yet to be fulfilled. Research efforts in the Metal Hydride Center of Excellence from the US DOE Hydrogen Program have been ongoing for more than a decade. In 2007, the prominent group narrowed down the list of promising elements to

produce an alloy that can meet the storage targets to the following: Boron, Lithium Magnesium and Nickel.

1.1 Research Scope

Although promising elements for metal hydrides have been identified, the experimental investigation of the hydrogen sorption properties of the alloys that exist within these four elements is a paramount task. In fact, when adding hydrogen to the list, the number of possible alloys that can be produced is 26 thus composed of 10 binary systems, 10 ternary systems, 5 quaternary systems and one with all five elements. Furthermore, once a system is chosen there are generally multiple phases that exist in that system. Since, all these phases react differently with hydrogen the overall situation results in a rather complex and time consuming experimental identification process for promising candidates. However, by combining experimental results from key samples with thermodynamic modeling the identification of promising compositions in a system can be achieved faster.

1.2 Research Objective

The objective of this work is to provide experimental data on key samples that is combined with thermodynamic modeling in order to predict compositions with favorable properties, such as enthalpy of formation. Therefore, the focus is placed on sample synthesis, sample characterization and hydrogen sorption testing. The system under investigation is Mg-Ni-H which was selected as it contains binary and ternary hydride phases while allowing to study the catalytic effect of Ni on Mg. Experimental investigation of this system is performed from 275°C to 400°C and hydrogen pressure ranging from 0-30 bar.

In the following chapter, information concerning the hydrogen storage methods under investigation in the literature and an in depth review of metal hydrides are given. Details on the experimental methods employed in this work are provided in Chapter 3. The following part, Chapter 4, discusses the experimental results of the Mg-Ni-H system. Finally, the summary and recommendations for future work are included in the last chapter.

Chapter 2

Literature Review

In order to subsist as an effective energy carrier, hydrogen needs to be stored easily and be readily available upon request. This section presents the available storage methods and compares their key parameters. In addition, thorough knowledge on metal hydrides is provided in order to identify the essential aspects of the method which is employed in this experimental work.

2.1 Hydrogen Storage Methods

There are six methods predominantly under investigation in the literature for hydrogen storage. They consist of compressed hydrogen gas, liquid hydrogen, physiosorption, metallic hydrides, complex metallic hydrides and chemical reactions.

2.1.1 **Compressed Gas**

The oldest form of storage used for hydrogen consists of compressing the gas. Currently, it is the most mature and commonly used technique to store hydrogen. This storage system is well adapted to stationary laboratory and industrial environments. However, in order to obtain large quantities in a small volume, as required for the transportation application, high compression is needed. In order to achieve the 2015 DOE storage target of 5.5 wt. %, involves reaching pressures in excess of 700 bar [10]. In addition, unlike ideal gases, hydrogen gas has a non-linear relation between pressure and volumetric storage capacity, as shown in Figure 2.1. Thus, as the pressure increases, a larger pressure increment is needed to achieve one unit increase in volumetric density.

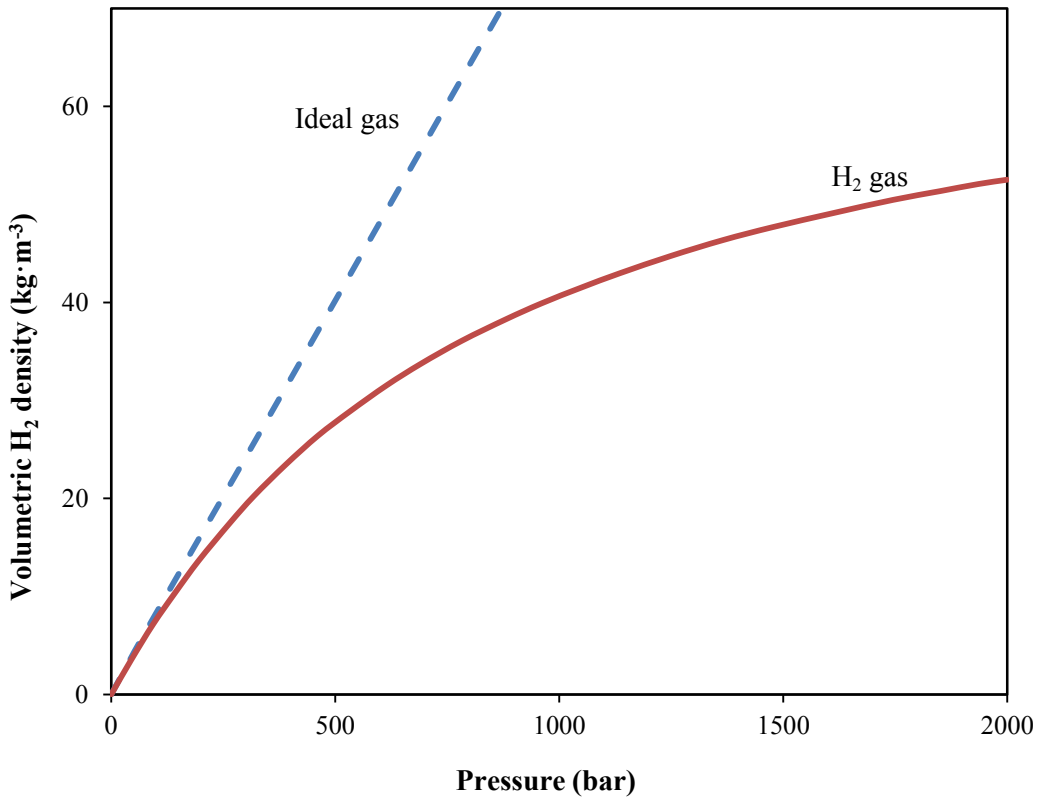

Figure 2.1: Compression curve hydrogen gas [10]

Such elevated pressures impose the use of advanced containment systems with high strength and low density. Typical high performance storage tanks are composed of several layers. These tanks are split up in four categories dependent on their pressure rating and safety rating. Type III is the one designed for light vehicle use. The inner portion of a type III tank is composed of a stress bearing layer made of light weight polymer carbon fiber composite. Moreover the outer layer typically consists of materials with high corrosion and mechanical resistance for safety purposes such as aluminum or steel alloys [11].

Although it is the simplest technique, compressed hydrogen storage has numerous drawbacks. Since hydrogen is stored under gaseous form, the safety concerns associated with the gas, such as ignition and detonation, exist in the event of an accidental release.

Moreover, the compressed gas method does not meet the 40 kg/m^3 storage target of the DOE. Although, the gravimetric storage performance of a 700 bar tank is 6.0 wt. % [12] the volumetric capacity is only 36 kg/m^3 [10]. Therefore, multiple tanks are required for automotive application, in order to obtain range similar to conventional vehicles, as seen with the 2010 Toyota Highlander FC which contains 4 storage tank at 700 bar with a range of 760 km [13]. Furthermore, pressuring hydrogen to such high pressure is a costly and complex procedure. Firstly, multiple compression stages are required in order to accomplish 700 bar. In addition, the high pressure ratios compression steps are inefficient, thus resulting in polytropic energy losses of 12-16% at 800 bar [10]. As a result, roughly 1/6 of the total energy content of hydrogen is consumed during the compression process. The research efforts in the compressed gas storage technique are focused on the storage tanks materials, manufacturing processes, heat transfer optimization and the safety aspects of high pressure hydrogen release [14-17].

2.1.2 **Liquefaction**

Another form of storage that has been employed for decades in industrial applications is the liquid storage, also known as cryogenic storage. Hydrogen exists in the liquid phase when its temperature is reduced below the critical temperature of 33.2 K [10], as shown in Figure 2.2. Liquid nitrogen is used to bring down the temperature of the hydrogen gas.

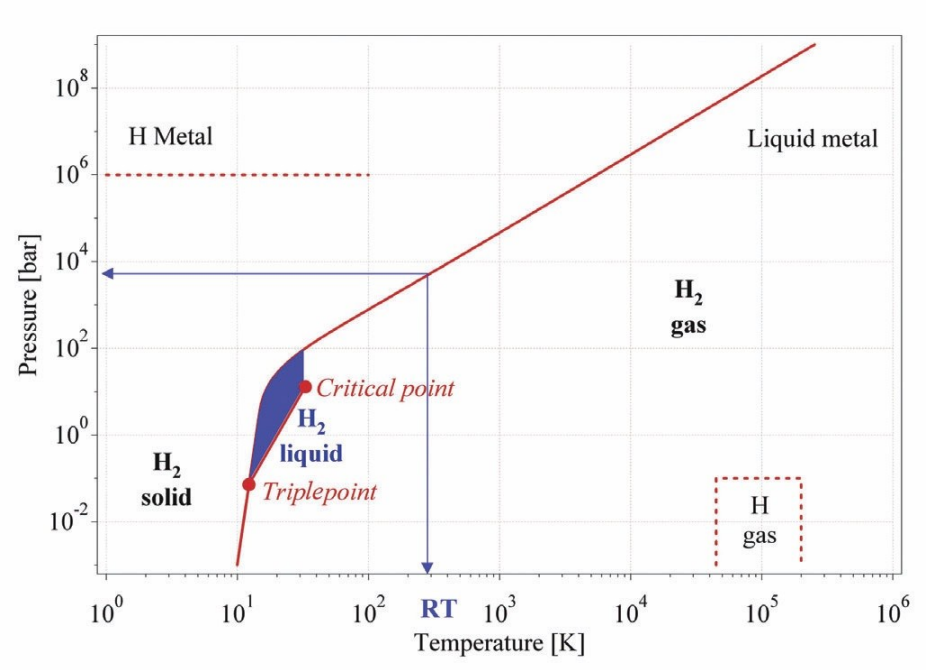

Figure 2.2: Hydrogen phase diagram [18]

This method offers respectively high volumetric and gravimetric capacities of 70.8 kg/m^3 and up to 20 wt. % depending on the size of the tanks [19]. During liquefaction, heat is released due the phase transition from ortho-hydrogen to para-hydrogen. This thermodynamic characteristic results in 25% of energy losses during the liquefaction process. Furthermore, the open hydrogen storage system used is subject to evaporation losses from heat transfer losses. For double-walled vacuum insulated spherical Dewar vessels, this boil-off effect results in 0.4% daily loss for a 50 m^3 system [19]. With the target being mobile automotive application, the liquid storage system suffers from complicated system requirements, weight issues and high costs. However, the technology is mature and fully operational concept units have been launched by manufacturers such as the 2006 BMW hydrogen 7. The ongoing research related to liquid storage is focused on high performance heat transfer materials [16].

2.1.3 **Physiosorption**

The third storage method is physiosorption, also known as adsorption, which consists of hydrogen molecules sticking onto the surface of a material through Van der Waals bonding, as illustrated in Figure 2.3. Due to the weakness of the interaction, hydrogen atoms can only form bonds with the surface at temperatures below 273 K. In fact, there is an exponential decrease in adsorption when temperature increases [20]. Since the temperature is never below the critical temperature of 33.2 K, the hydrogen remains under gaseous phase throughout the process [21]. Therefore, the storage process taking place is described as a monolayer adsorption mechanism. Thus, the adsorption capacity is heavily dependent on the specific surface area of the storage material [22]. For porous substrates, the surface adsorption is accompanied by hydrogen atoms squeezing in the void space [23].

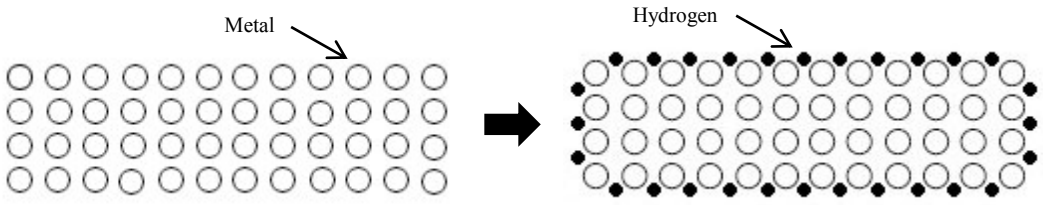

Figure 2.3: Adsorption schematic

One of the advantages of this method is the low operating pressure. In addition, the hydrogen boil off losses encountered with liquid storage is replaced with nitrogen evaporation which is used to cool the substrate. Furthermore, both the nitrogen cooling and the materials used as substrates have relatively low cost [21]. However, the low gravimetric storage (< 6 wt. %) is a drawback for transportation usage [24, 25]. There are numerous research topics related to physiosorption, which include storage materials and their geometry as well as manufacturing techniques [26].

2.1.4 **Metal Hydrides**

The fourth method is metal hydride storage. Here, hydrogen is stored via chemical bonding between hydrogen and the metallic atoms to form a new compound also known as hydride phase. Figure 2.4 presents a schematic view of the process. The reaction takes place at specific temperature and pressure values which are material dependent characteristics. The hydride formation reaction can be represented by the following equation:

$$H_2 + M \leftrightarrows MH_x + E$$

where M is a metal (alloy or pure element) and MH_x is the obtained hydride. The absorption reaction is exothermic thus resulting in the desorption reaction being endothermic.

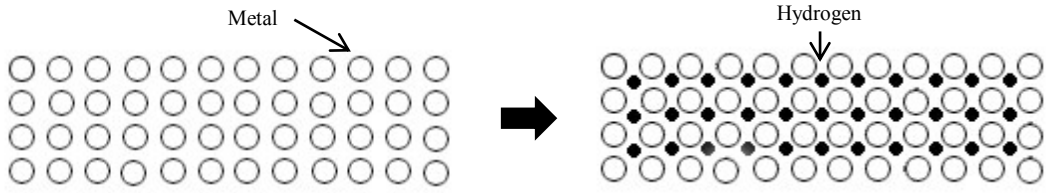

Figure 2.4: Absorption schematic

This storage method offers a long life as some powdered samples can undergo several hundreds of charging and discharging cycles while maintaining storage performance, as shown with $Ni_{64}Zr_{36}$ [27]. The volumetric storage capacity from metallic hydrides is high, in the range of 70-150 kg/m^3 [10]. However, the gravimetric capacity is low, 1-7.6 wt % [28]. In addition, thus far the discovered metals that offer large storage capacity have slow kinetics while those with fast kinetic offer limited storage capacity [25]. Moreover, the alloys currently selected for demonstration projects include costly rare elements such as Lanthanum in $LaNi_5$ [29]. Currently, there is no metal hydride that

meets the DOE 2015 requirements of 5.5 wt. % and 40 kg/m^3 for mobile applications [30].

2.1.5 **Complex Hydrides**

Complex hydrides behave in a similar manner to metallic hydrides. However, the main difference concerns the hydride phases formed that are of ionic or covalent nature. In other words, the bonds formed are more stable. Complex hydrides present high gravimetric capacity of 18.5 wt. % $LiBH_4$ [31] and high volumetric capacity 121 kg/m^3 $LiBH_4$ [32]. However, the stable nature of the complex hydrides makes it difficult, yet often impossible, to release the stored hydrogen. Compounds that can release hydrogen require elevated temperature in the range of 70-650°C [30, 33]. Furthermore, the release of hydrogen takes place in cascade reactions that possess different optimal operating conditions [34]. In addition, the desorption process often creates products different from the starting material, such as NH_3 [31]. Moreover, these products act as impurities and pose issues for the cycling ability of the material [31]. At the moment, there is no complex hydride capable of absorbing and desorbing high purity hydrogen that meets the 2015 DOE targets of 5.5 wt. % and 40 kg/m^3 [35, 36].

2.1.6 **Chemical Reactions**

The last storage method is chemical reactions which also includes chemical compounds. The redox reaction between some metals or chemical compounds with water generates hydrogen. These reactions are not directly reversible. They require an additional reduction reaction in order to obtain the starting reactants, as seen with the reaction sequence below.

Reaction 1 $2\ Na + 2\ H_2O \rightarrow 2\ NaOH + H_2$

Reaction 2 $2\ NaOH + 2\ e^- \rightarrow 2\ Na + 2\ OH^-$

The process is limited to low gravimetric and volumetric capacities which basically consist of hydrogen molecules contained in water. In addition, high temperatures are required for the reduction reactions [37]. The process is safe, stable and cost effective for solar furnaces applications [38]. However, this technique is not feasible for transportation uses as it requires power plant size installations [39].

In addition, Hydrogen can also be stored inside chemical compound such as methane (CH_4), ammonia (NH_3) and many others. Surprisingly the gravimetric and volumetric performance of these compounds meet DOE targets. However, substantial energy is require to break the stable covalent bonding in the molecules, not to mention the complex purification process needed to isolate the hydrogen gas. Thus, on-board treatment of chemical compounds is not viable for mobile applications.

2.1.7 **Summary**

Six methods of storing high purity hydrogen have been described. These consist of compressed hydrogen gas, liquid hydrogen, physiosorption, metal hydrides, complex hydrides and chemical reactions. Each method faces numerous challenging aspects for mobile applications for instance weight, size, cost and durability. As a result, at the moment none of the candidates offer an overall package that meets the 2015 DOE targets of 5.5 wt. % and 40 kg/m^3 while offering operating parameters that are compatible with mobile transportation applications. In addition, the situation is gloomy when considering that the ideal objective is eventually to surpass the hydrogen storage capacity of liquid gasoline at 15.8 wt. % and 112 g/L [31]. Figure 2.5 summarizes the storage performance

of the compressed gas (red, dashed line), liquid (navy blue, dashed line), physiosorption (black, dotted line), metal hydrides (purple, diamond), complex metal hydrides (light blue, square), chemical compounds (orange, circle) and DOE targets (green, dash-dotted line).

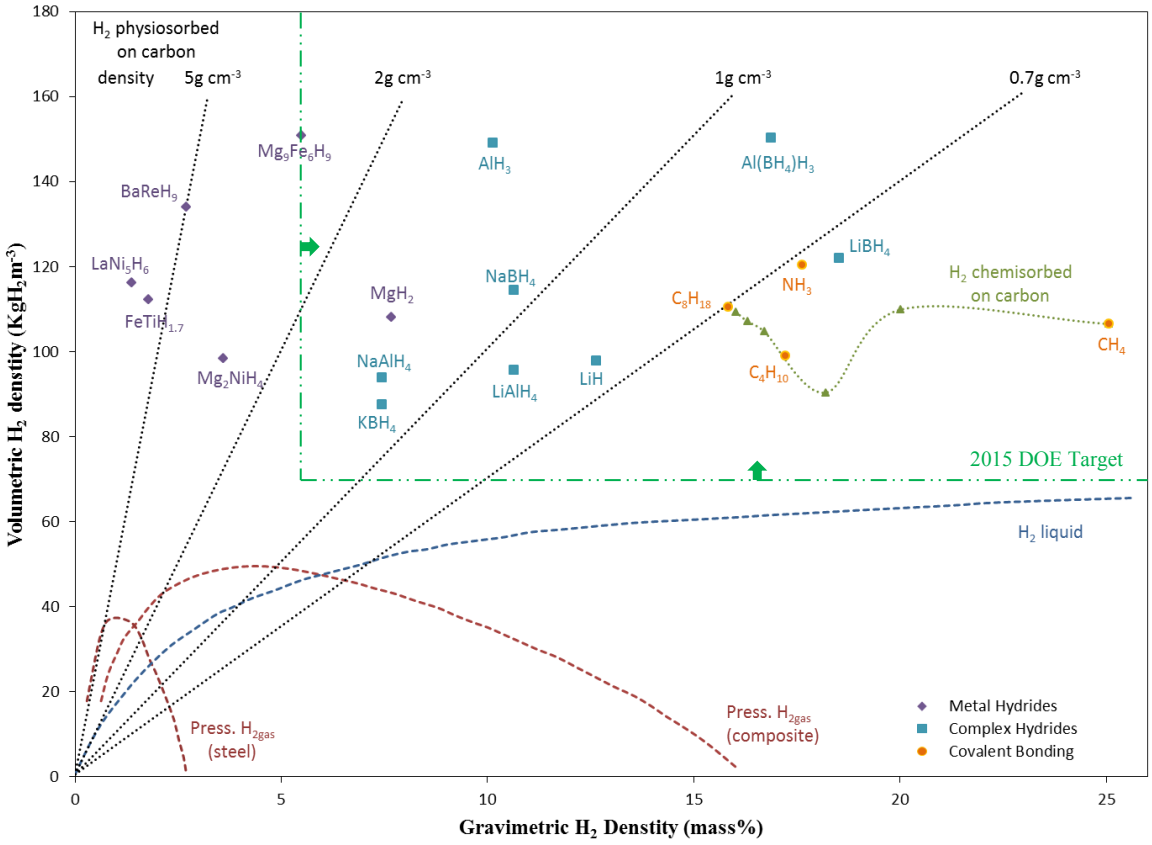

Figure 2.5: Volumetric and gravimetric density of selected hydrides [40]

2.2 Hydrogen Interaction with Metals

Metal hydrides stand out amongst the list of promising candidates for commercial hydrogen applications due to their overall storage performance and their simple refueling. However, elevated operating temperatures and slow kinetics prevent the broad adoption of the technology. Improving the characteristics therefore requires a survey of the

elemental understanding of the interaction between metals and hydrogen from a number of fields such as chemistry and physics to identify areas of potential improvement.

From a chemical viewpoint, the list of elements that react with hydrogen and form hydrides is quite extensive, as shown in Figure 2.6. In fact, out of the 118 confirmed elements only 30 do not form hydride phases. From this number, 24 are metallic elements and the remaining six are the noble gases. Interestingly, this rather general observation subtly indicates the unique character of the atomic bonding between metals and hydrogen. Eleven of the metallic elements that do not interact with hydrogen consist of either radioactive elements or rare elements with no stable isotopes, thus obtained either from decay reactions or synthetically (Fr, Ra, Pm, Cm, Bk, Cf, Es, Fm, Md, No, Lw). The remaining 15 metallic elements that do not form binary hydrides fall into the columns 6 to 11 of the periodic table and are referred to as the "hydride gap" [41].

1	2	3	4	5	6	7	8	9	10	11	12	13	14	15	16	17	18
H 2.20																	He
LiH 0.97	BeH_2 1.47				Ionic		Metallic					BH_3 2.01	CH_4 2.5	NH_3 3.07	H_2O 3.50	HF 4.10	Ne
NaH 1.91	MgH_2 1.23				Covalent		Intermediate					AlH_3 1.47	SiH_4 1.74	PH_3 2.06	H_2S 2.44	HCl 2.83	Ar
KH 0.91	CaH_2 1.04	ScH_2 1.20	TiH_2 1.32	VH VH_2 1.45	CrH CrH_2 1.56	Mn 1.60	Fe 1.64	Co 1.70	$NiH_{<1}$ 1.75	CuH 1.75	ZnH_2 1.66	(GaH_3) 1.82	GeH_4 2.02	AsH_3 2.20	H_2Se 2.48	HBr 2.74	Kr
RbH 0.89	SrH_2 0.99	YH_2 1.11	ZrH_2 1.22	NbH NbH_2 1.23	Mo 1.30	Tc 1.36	Ru 1.42	Rh 1.45	$PdH_{<1}$ 1.35	Ag 1.42	CdH_2 1.46	(InH_3) 1.49	SnH_4 1.72	SbH_3 1.82	H_2Tc 2.01	HI 2.21	Xe
CsH 0.86	BaH_2 0.97	LaH_2 LaH_3 1.08	HfH_2 1.23	TaH 1.33	W 1.40	Re 1.46	Os 1.52	Ir 1.55	Pt 1.44	(AuH_3) 1.42	(HgH_2) 1.44	(TlH_3) 1.44	PbH_4 1.55	BiH_3 1.67	H_2Po 1.76	Hat 1.90	Rn
Fr	Ra	AcH_2 1.00															
			CeH_3 1.05	PrH3 PrH_2 1.07	NdH_2 NdH_3 1.07	Pm	SmH_2 SmH_3 1.07	EuH_2 1.01	GdH_2 GdH_3 1.11	TdH_2 TdH_3 1.1	DyH_2 DyH_3 1.1	HoH_2 HoH_3 1.1	ErH_2 ErH_3 1.11	TmH_2 TmH_3 1.11	(YbH_2) YoH_3 1.06	LuH_2 LuH_3 1.14
			ThH_2 1.11	PaH_2 1.14	UH_2 1.22	NpH_2 NpH_3 1.22	PuH_2 PuH_3 1.22	AmH_2 AmH_3 1.2	Cm	Bk	Cf	Es	Fm	Md	No	Lw	

Figure 2.6: List of elements forming hydrides and their electronegativity [7]

On the other hand, there are 33 metallic elements that form hydrides. Moreover, these hydrides are divided into the following four categories: ionic hydrides, metallic hydrides, covalent hydrides and intermediate hydrides. The ionic or salt-like hydrides possess a crystal structure that shows an ionic lattice, thus containing the negatively charged H^- ion. The metallic or interstitial hydrides maintain some metallic properties such as hardness, their ability to conduct electricity and their magnetic properties. Covalent hydrides are typically formed between non-metals and hydrogen, in which the bonds are electron pairs shared by atoms of comparable electronegativities. Finally, the intermediate hydrides have a mix of properties from both metallic and covalent hydrides.

The classification of hydrides provides an insight on the different mechanism of hydrogen storage in metals. In effect, the infiltration of hydrogen inside a metal is named absorption or chemisorption. Although the first metal hydride was reported by Graham (1887), the two step mechanism currently used to describe the process was established by Smithells (1934) [42]. The first stage involves the dissociation of the hydrogen molecule into single atoms at the surface of the metal; and the second consists of the subsequent diffusion of these hydrogen atoms into the interstitial positions of the metal's lattice.

The separation of hydrogen into single atoms is dependent on the electronic properties of the element(s) for instance electronegativity. Nonetheless, it is important to note that other aspects such as crystal structure have an indirect impact on the electronic behavior and therefore play a role in the dissociation characteristics of the metal [43]. Additionally, in the case of alloys, the variation of elements within the composition range of a particular phase modifies the electronic cloud, thus modifying the surface's

electronic dissociation properties [44]. As a result, different compositions within a metallic system will breakdown hydrogen molecules into single atoms at distinct rates.

The dissociated hydrogen atoms enter the metals by initially filling the large empty spaces such as defects, voids and grain boundaries. It is important to note that the size of these openings is considered large with respect to a single hydrogen atom which has the smallest atomic radius of all elements at 25 picometers [45]. However, the storage due to large space filling is rather negligible in comparison with the total amount of hydrogen stored in the metal.

In fact, the greater part of the hydrogen stored inside metals takes place through interstitial storage. Given that the atomic size ratio between hydrogen and any metallic element is significantly greater than 15%, hydrogen atoms cannot substitute for the metallic atoms' positions in the crystal structure [46]. Hence, the diffusion process that takes place can only be of interstitial nature. At first, the most energetically favorable positions are filled. Afterwards, the hydrogen atoms penetrate deeper by jumping from one vacant interstitial position to the next. The introduction of the hydrogen atoms in the interstitial position increases the volume of the lattice [47]. As a result the hydride phases have larger lattice parameters that the original metallic cell. Examples of pure interstitial metal hydrides are Palladium, Titanium and Niobium [48].

On the other hand, in some instances the resulting hydride phase consists of interstitially diffused hydrogen atoms in a rearranged metallic phase. Thus, the re-organization of the metal's atomic arrangement is known as a phase transformation. Metals that adopt such mechanism for hydrogen uptake are termed transformation

hydrides. Magnesium, Calcium and Copper are examples of elements that form transformation hydrides [49-51].

The diffusion of hydrogen atoms inside a metallic phase is exponentially faster than the diffusion of these atoms inside a hydride phase [52, 53]. This can be explained by the reduced mobility of the hydrogen atom when the surrounding interstitial spaces are partially occupied. As a result, the diffused hydrogen atoms act as impurity atoms for the following hydrogen atom. Moreover, since the most favorable positions are filled at first, the subsequent ingoing hydrogen atoms require higher energy to fill the less favorable sites, thus also slowing down the diffusion process [54, 55]. Therefore, as the hydride phases form, the hydrogen takes more time to reach the core region of the grains. This aspect of metal hydrides is often the rate limiting step for hydrogen diffusion. Hence, hydrogen absorption in metals emerges as a grain surface phenomenon, as seen in the nucleation sites in Figure 2.7 and Figure 2.8 [56, 57].

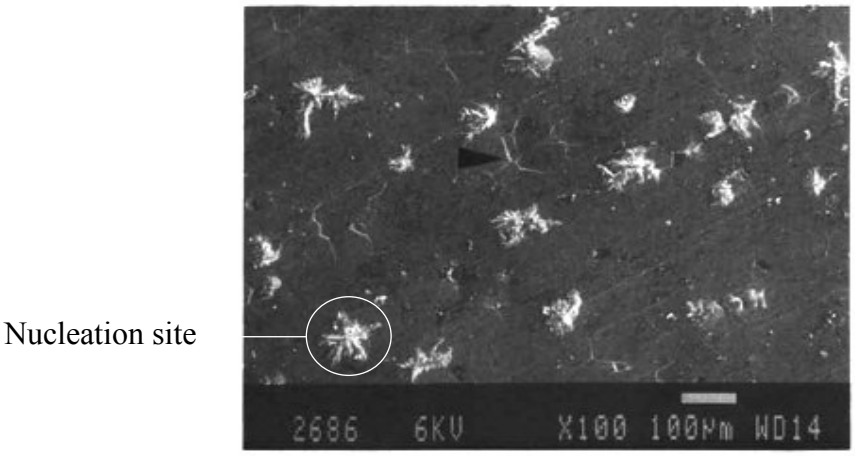

Figure 2.7: SEM image Mg thin foil 15% hydrided [56]

Moreover, the average thickness of this formed hydride layer is approximately 10-100 micrometers [19, 57]. Not only does this aspect play a crucial role when optimizing

the materials performance but it also has a significant impact on the synthesis and characterization of samples. When the sample particle size diameter is in the region of 100 micrometer, two distinct regions are found in the sample: the surface layer consisting of the hydride phase and the core region of the particle which contains only metallic phases [58], as shown in Figure 2.8. This aspect plays a role in the optimization of the kinetics of a material [59-62].

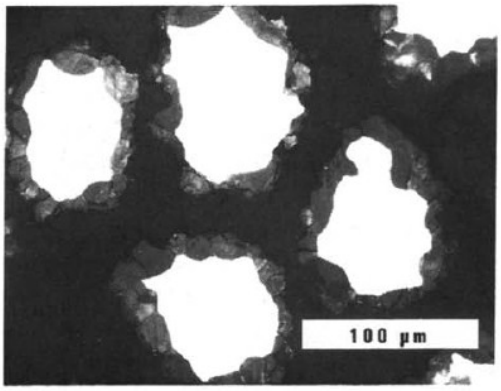

Figure 2.8: SEM image Mg particle at 400°C and 20 bar H_2[57]

With the hydrogen stored in the metal, the ensuing step in the description of the interaction consists of the release of the hydrogen atoms. Also known as desorption, the endothermic hydrogen discharge process takes place when the applied pressure is reduced below the equilibrium absorption pressure of the metal and heat is applied [10]. At that point, hydrogen atoms escape the interstitial positions in the lattice and recombine at the surface to form hydrogen molecules [63]. As a general rule, some hydrogen atoms remain trapped inside the metal due to defect and voids even when the pressure is reduced to vacuum due to high binding energy of some atoms [44, 64].

2.2.1 Thermodynamics

The above described mechanism of hydrogen interaction with a metal is heavily dependent on the thermodynamic properties of the sample. In fact, thermal energy is required to overcome the activation barrier for the formation of hydride phases. The temperature needed for hydrogen absorption varies for different metallic elements and alloys.

On the other hand, the change in entropy that occurs is mainly derived from the phase change from molecular hydrogen gas to dissolved solid hydrogen [10]. As a result, the entropy change can be approximated by the standard entropy of hydrogen S^o = 130.684 $J \cdot K^{-1} mol^{-1}$. Therefore, the entropy of formation ΔS_f is -130.684 $J \cdot K^{-1} mol^{-1}$ for all metal hydrogen systems [10]. Consequently, during the absorption process since the hydrogen dissolves into the solid, thus gaining more order, the entropy of the system decreases and the excess is released as heat. Conversely, during desorption when the solid hydrogen escapes into hydrogen gas, the same quantity of heat is required which explains the endothermic nature of desorption.

$$\Delta Q = T \cdot \Delta S \qquad \textbf{\textit{Equation 2.1 Heat Evolution}}$$

The enthalpy of formation of metal hydrides (ΔH_f) describes the stability of the metal-hydrogen bonds. This thermodynamic property relates to the disposition of the metal to release the stored hydrogen. Changes in ΔH and ΔS are related at the equilibrium pressure through the Van't Hoff equation [65].

$$ln\left(\frac{P_{eq}}{P_{o\ eq}}\right) = \frac{\Delta H}{R} \cdot \frac{1}{T} - \frac{\Delta S}{R} \qquad \textbf{\textit{Equation 2.2 Van't Hoff}}$$

The above equation is used to obtain Van't Hoff plots. They are commonly used to present the stability of metal hydrides for comparison purposes, as shown in Figure 2.9

which includes the Van't Hoff plots of key metal hydrides. The more stable hydrides appear on the left and the least stable on the right.

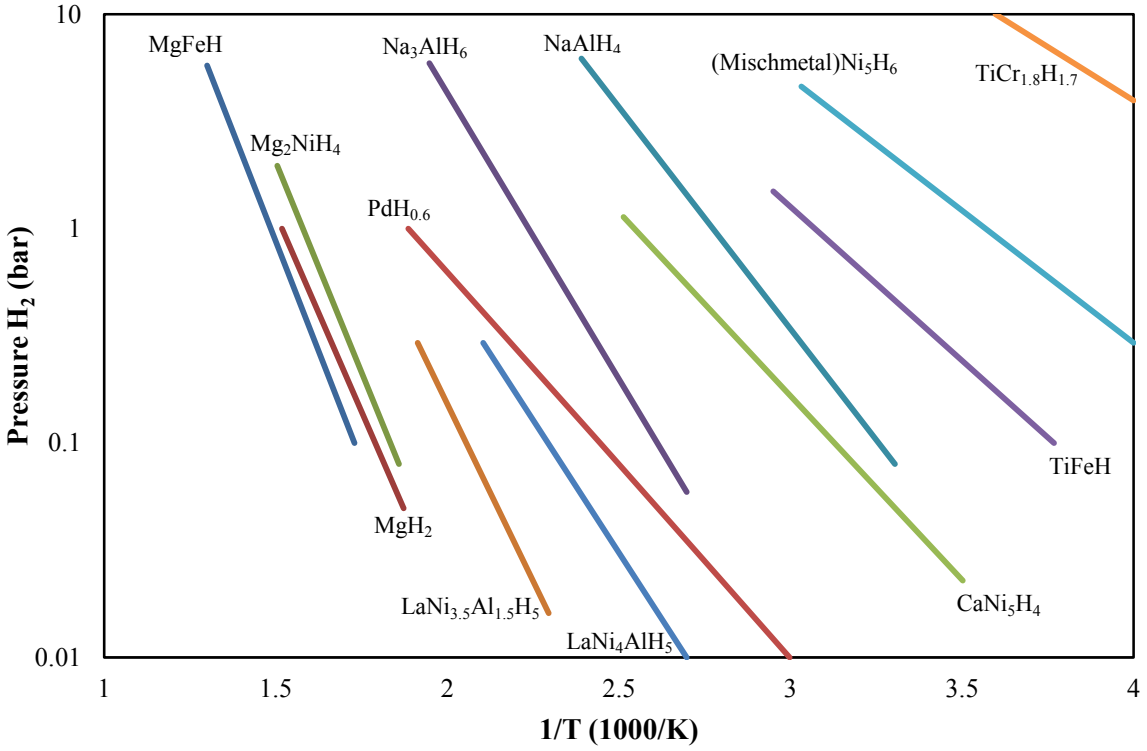

Figure 2.9: Van't Hoff plot of common metal hydrides

2.2.2 Pressure

The second key parameter that governs the hydride phase transformation is pressure. Pressure is known as the driving force behind the hydrogen absorption. By elevating the pressure, there is an increase of the hydrogen species concentration in the free gas. Consequently, there is an increase in the concentration gradient between the gaseous hydrogen and the hydrogen atoms inside the metal. Fick's first law shows that the flux is proportional to the concentration gradient and the diffusion coefficient (D, cm^2/s). Therefore the increase of pressure results in faster diffusion speed of the hydrogen ions inside the metal. Thus, supporting the concept of driving force commonly attributed to pressure.

$$J = -D\nabla\frac{\partial\varphi}{\partial x}$$ ***Equation 3 Fick's First Law***

However, there exist two distinct pressure values during the hydrogen absorption process. The first consists of the pressure inside the chamber or external gas pressure which ranges experimentally from 0.1 to 50 000 bar [66-68]. The second, is the pressure of the hydrogen atoms inside the metal also known as thermodynamic pressure which is above $1x10^6$ bar [48]. Interestingly, the thermodynamic pressure is of the order of the pressure required to form solid hydrogen which is theoretically established at $3.4\ x10^6$ bar [69] as shown in Figure 2.2. Although thermodynamic pressure is of importance for theoretical approaches such as modeling, it is more useful to link the external pressure to the hydrogen concentration at the surface of the metal, which in turn affects the chemical potential of the reaction [47, 70]. Thus, pressure values communicated in the literature predominantly describe the external gas pressure.

In addition, when this applied pressure is in the range of 1000 - 50 000 bar high pressure hydride phases are formed [47]. The high pressure hydrides phases present a structure different from the more common low pressure hydrides [71, 72]. In fact, the interstitially located hydrogen atoms are packed much closer in high pressure hydrides and therefore multiple hydrogen atoms are found in one interstitial region. On the other hand, high pressure hydride phases are often metastable and have high desorption pressures making them impractical for application purposes [67]. Nonetheless, in some rare instances high pressure hydride phases present reversible hydrogen sorption properties such as $Mg_{0.82}Zn_{0.18}H_2$ [73]. Hence, research on high pressure hydrides contributes mainly to fundamental concepts as opposed to applications.

2.2.3 Composition

Another key parameter for hydrogen storage is the composition of the alloys. In fact, two situations arise, the first when the change in alloying elements is within the boundaries of a phase and the second when the change of composition produces a new phase, thus outside the limits of the initial phase. In the former instance, the hydrogen storage properties of the alloy are minimally altered, although the surface dissociation capacity is affected due to the modification of the electronic configuration of the alloy. In the latter situation, the hydrogen absorption characteristics are significantly different due to the change in microstructure and atomic structure between the two phases.

Nonetheless, alloying is used to tailor the absorption characteristics of a certain element [19]. Thus, the alloy comprises one element with high hydrogen storage capacity while the other element(s) are added to serve as catalysts which improve the kinetics of the reaction. An example is the Mg-Ni system which utilizes the catalyst strategy. When as little as 5% of Ni is added, the Mg is destabilized and the time needed for desorption is reduced from hours to minutes [59, 74, 75].

2.2.4 Crystal Structure

The role of atomic arrangement in hydrogen storage is intricate. In reality, since it is impossible to change the crystal structure of a material while maintaining all other properties constant, understanding the role of atom arrangement in hydrogen absorption is an elaborated problem. Intuitively, it is expected that the atomic structure with the lowest atomic packing factor should allow for the highest storage capacity due to their larger interstitial space. However, this does not apply as a rule to all metal-hydrogen systems. In some instances, the Face-Centered Cubic (FCC) or Hexagonal Close Packed

(HCP) structure of a system stores more hydrogen than the Body-Centered Cubic (BCC) phase of the system, although the first two have a packing factor of 0.74 whereas the cubic has only 0.68 [43, 46].

The feature of atomic arrangement that is more informative is the effect of crystal ordering on hydrogen storage. Unlike the crystal structure, the level of order can be modified while maintaining the composition of the sample. Yet still, no clear understanding of the atomic ordering effect on hydrogen storage has been identified so far. In some instances the crystalline sample stores more hydrogen than its amorphous counterpart, while the opposite situation takes place for other systems. Then again, numerous material properties that depend on the atomic arrangement such as electronic configuration are not preserved between the two samples. Furthermore, short range ordered and metastable metals are areas of research by themselves. Therefore, proper understanding of their interaction with hydrogen suffers from the lack of knowledge on their basic properties. Nonetheless, one identified advantage of amorphous structured materials is the improved resistance to pulverization during hydrogen cycling experiments when compared to crystalline samples [76]. This behavior is in part due to the improved mechanical properties of amorphous structures such as yield strength and ductility [27].

2.3 Metal Alloying Techniques

In order to offer optimal performance, metals capable of absorbing hydrogen require high purity. Bulk or surface impurity atoms change the electronic configuration of the sample and therefore hinder the diffusion of hydrogen atoms. For example, surface oxidation considerably increases the number of cycles needed to activate the sample and in some

systems it can make activation impossible to achieve [77]. Therefore, all techniques employed to produce the starting alloys operate under controlled environment. The alloying methods used to produce samples for hydrogen sorption experiments include melting and mechanical alloying. The melting processes are completed in induction furnaces [78-80], arc melting furnaces [81-83] and vacuum furnaces [84]. Mechanical alloying techniques are achieved by ball milling [85-87] and rolling [88-90].

The above mentioned methods generate samples in equilibrium state also known as crystalline metals. The non-equilibrium structures such as amorphous materials are obtained via other methods such as extended ball milling [91-93] , sputtering [94] and rapid quenching techniques for instance melt spinning [95-97] and injection casting [98].

2.4 Metal Hydride Synthesis

There are two methods available to introduce hydrogen in metals. The first method produces hydrides by a process called electro-chemical testing. The alloy of interest is fabricated as an electrode which is submerged in a basic solution such as potassium hydroxide (KOH) [95]. Current is then passed through electrode. This electrical energy causes the dissociation of hydrogen ions from the molecules of the solution. Since the reaction takes places at the surface of the electrode, the released hydrogen can then penetrate the metallic electrode. In addition, the strong electron flow promotes the motion of the hydrogen ions inside the metal. The hydrogen storage capacity of the metal is related to the specific current density flowing through the metal (mA/g). Nonetheless, the exact amount of hydrogen stored is verified using a high precision scale. Furthermore, the desorption characteristics of the material require additional equipment as it cannot be

carried out electro-chemically. The advantages of this technique are that the experiments are performed at room temperature and the testing equipment is simple.

The second method is named the volumetric method. It consists of heating a metallic sample to its required activation energy and exposing it to hydrogen gas pressurized up to 200 bar. This pressure range represents typical operating parameters of commercial testing equipment. In addition, two methods are used to monitor in situ the amount of stored hydrogen. The first employs accurate force measurement which allows to capture minute changes in the weight of the sample. This approach is known as the gravimetric method or thermal gravimetric analysis (TGA) [99, 100]. On the other hand, the second technique makes use of precise hydrogen pressure measurements in a chamber with calibrated volume [97, 101]. Also known as Sievert type apparatus, it makes use of the ideal gas law to calculate the amount of stored hydrogen by monitoring closely the pressure drops in the chamber.

The experimental data obtained by the volumetric testing methods is presented through a plot of pressure and hydrogen content which is named pressure composition isotherms (PCI). An example of the representation of the formation of MgH_2 is shown in Figure 2.10. It can be seen during the absorption and desorption steps that at a certain pressure the hydrogen concentration is changing while the pressure remains constant thus resulting in the distinctive “plateau” equilibrium region for transformation hydrides. At pressures below the plateau, during absorption, the sample undergoes random interstitial position filling by hydrogen atoms which results in a disordered solution [64]. Some researchers [102, 103]identify the desorption reaction as the equilibrium. However,

theoretical [104] and experimental [105] findings indicate that the equilibrium is halfway between the absorption and desorption isotherms, in terms of chemical potential.

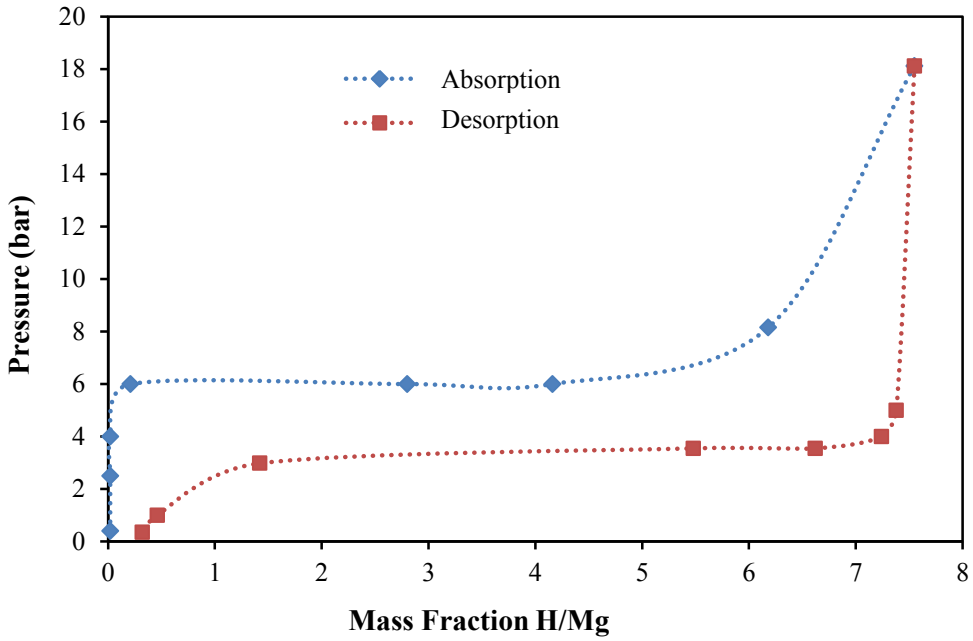

Figure 2.10: PCI absorption and desorption Mg + H_2 at 350°C [106]

In addition, the plot also shows a characteristic feature of metal hydrides which consists of a pressure difference between the absorption and the desorption plateau known as hysteresis. Hysteresis is linked to the plastic work that occurs during the formation and decomposition of hydride phases [107]. In more general terms, the hysteresis of a hydride sorption reaction is proportional to the ratio of free energy of the absorption and desorption reaction [108]. This aspect plays a crucial role in practical applications as a large hysteresis substantially increases the cost and complexity of the hydrogen storage unit.

Moreover, the PCI plots provide information on the phase boundaries contained in phase diagrams. In fact, at a fixed pressure the PCI data can be linked to the solubility of phases at the temperature of the isotherm. This connection is essential for the

development of hydrogen storage alloys. Furthermore, thermodynamic modeling reduces the amount of experimental work required to establish the extent of the various phases over the full composition range.

The PCI curves also represent the theoretical equilibrium hydride formation for an alloy. However, experimentally a surface oxide layer is present which requires activation cycles before stable and repeatable results are obtained. The activation consists of several cycles of exposure of the sample to high hydrogen pressure and high temperature. This causes the uniform oxide layer to breakdown into more stable oxide clusters which exposes an unreacted surface of the sample. In addition, the initial hydride phase formation causes extensive cracking and decrepitation of the metallic sample which is pulverized into a fine powder. This grain size refinement is due to the great amount of stress induced by the large volume expansion by the interstitial hydrogen atom which ruptures the crystals [109-111]. The volume increase can reach more than 10% in some systems [112]. Consequently, depending on the systems anywhere from one to ten activation cycles each lasting hours to days are typically required before reaching repeatable equilibrium hydride formation experimentally, as shown in the experimental results section of this work.

Another important parameter for PCI tests is the minimum pressure during desorption, also referred to as lower limit. Experimentally, the lower the minimum pressure the more hydrogen can be released from the sample. Therefore depending on the reversibility of a system different lower limits are used in the literature, thus making it difficult to compare the performance. However, in a real life system for commercial applications the lower limit is fixed by the design and operation conditions of the system.

For example, an automotive hydrogen fuel cell supplied by solid state storage would have a minimum desorption pressure for 2 to 5 bar [113] due to the fuel cell operation requirements. The lower limit pressure for desorption is rarely if not ever taken into consideration or reported in the literature although it plays a crucial role in the performance of real applications.

2.5 Sample Characterization

Sample characterization is at the core of experimental investigation of materials for metal hydrides application. In fact, due to the limited theoretical understanding, the majority of the information found in the literature focuses mainly on the systematic characterization of metal hydrogen systems. A variety of tools are used to perform the experimental investigations. X-ray diffraction (XRD) is employed primarily for phase identification and also to study the crystallographic structure evolution during hydrogen sorption cycling. Powder diffraction is suitable for hydrogen sorption samples which remain under fine powdered form throughout the experimentation. However, low atomic number elements such as hydrogen are invisible to X-rays due to low number of electrons that can interact with the X-ray beam. Therefore, detailed study on the hydrogen atoms cannot be performed with the XRD. Instead, another diffraction technique used is neutron diffraction. Unlike the XRD, hydrogen and hydrogen isotopes strongly diffract neutrons[114]. Thus, hydrogen positioning in a crystal structure can be precisely determined. In addition, precise information regarding metal lattice constants can be obtained from neutron diffraction.

Microscopy is another key tool used in the characterization of hydrogen-metal interaction. Optical microscopy is seldom performed since ingot style samples are rarely

employed. However, earlier published papers from the 1980s report some optical micrographs [57]. Scanning electron microscopy (SEM) is commonly implemented as it can provide detailed microstructure information on powder samples [115]. Transmission electron microscopy (TEM) is also used to investigate the atomic arrangement and crystallite size [74, 75, 88].

Thermodynamic data on the metallic phases is experimentally obtained through differential scanning calorimetry (DSC) and thermogravimetric analysis (TGA). On the other hand, thermodynamic information on hydrogen absorption and desorption is achieved by pressure differential scanning calorimetry (PDSC) experiments [106, 116, 117]. The pressure range of PDSC units is limited to 10 bar and the accuracy of pressure measurements is low. Thus, although it can provide some thermodynamic data little conclusions can be made solely on that information which explains the limited usage of the method in the literature. Conversely, desorption thermodynamic data from thermal desorption spectroscopy (TDS) [78], DSC [86] and TGA [118, 119] is more readily available with satisfactory accuracy.

2.6 Mg-H Binary System

The reaction between hydrogen and pure magnesium produces an intermediate type hydride named magnesium hydride (MgH_2). The high gravimetric and volumetric hydrogen storage capacity, respectively, 7.6 wt. % and 115 kg/m^3 of MgH_2 explain the vast amount of research on the system for mobile applications [120]. Direct hydrogenation of magnesium was first performed by Wiberg & Bauer in 1951 [121]. Subsequently, crystal structure information was gathered in 1955 [122]. Since then, efforts have been made to accelerate the slow desorption kinetics of MgH_2 and to reduce

the equilibrium temperature which is 288°C at 1 bar pressure [123]. The elevated desorption equilibrium temperature of MgH_2 is the consequence of the high thermodynamic stability of the hydride which is reflected by its ΔH of -75 kJ/mol H_2 [124-126].

Two methods are employed to improve the kinetics of the hydrogen sorption. The first is the minute addition of alloying elements such as Ti, V, Mn, Fe, Co, Ni, Cu, Pd that play a catalyst role [127-135]. The second approach consists of nano-scale grain refinement through ball milling. In practice, the two techniques are performed together since alloying is predominantly carried out using the mechanical alloying process. Yet still, both techniques drastically improve the kinetics of the hydrogen absorption and desorption in magnesium alloys. These methods also impact the temperature required for the hydrogen absorption. However, the reduction in temperature is small and often negligible since the reduction of ΔH is accompanied by an increase of ΔS thus cancelling out the potential thermodynamic gain in Van't Hoff equation [136].

More recently, MgH_2 is used to produce "reactive hydride composites" such as $LiNH_2/MgH_2$ [137, 138] and $LiBH_4/MgH_2$ [139]. This type of material aims at combining the advantages of metal hydrides and complex hydrides such as high reversibility and high storage capacity.

2.7 Ni-H Binary System

No low pressure hydride phase is contained in the system, thus making the Ni–H phase diagram rather simple. In fact, only limited hydrogen solubility is found in nickel [140]. However, a high pressure hydride phase (β-NiH_{1-x}) exists for the Ni-H system at a hydrogen pressure of 1600-1900 bar when heated to 400°C or 6000 bar when tested at

25°C [141, 142]. Nonetheless, these pressure ranges are beyond the scope of the present study and therefore, the hydride β- NiH_{1-x} is not included in this work.

2.8 Mg-Ni-H Ternary System

The Mg-Ni-H is the most investigated magnesium based alloys system for hydrogen storage. The interest in the system is associated with the catalytic effects of Ni on Mg which reduces desorption kinetics from hours to minutes. The system was first studied experimentally by Reilly and Wiswall in 1968 [143]. The system contains one binary hydride MgH_2 and one ternary hydride Mg_2NiH_4 obtained from the reaction between the intermetallic Mg_2Ni and H_2 [143, 144]. As little as 5% (atomic %) of Ni is needed to enhance the desorption kinetics from over one hour to less than 10 minutes under 1 bar desorption pressure.

The interest for the system also comes from the fact that it is one of the first systems where the benefits of mechanical alloying through nano-crystals were obtained [87]. More recently, a number of stable high pressure ternary hydrides have been discovered such as $MgNi_2H_{3.2}$ at [145], $MgNi_{1.02}H_{2.2}$ [146], $Mg_2Ni_3H_{3.4}$ [147, 148], Mg_2NiH_4 [149]. Although the kinetics of the hydride reactions in the system meet commercial requirements, the operating temperature for the absorption and desorption in the Mg-Ni-H is around 220°C [119] which remains too elevated for vehicular applications.

The information surveyed on metal hydrides has shown that the method presents good potential for commercial applications. In fact, metal hydrides provide good reversibility, simple system operation along with excellent volumetric and gravimetric storage. However, up to now metal hydride system possessing all of the required

characteristics at once has not been found. Although the literature on metal hydrides is vast, research efforts are still required for tailoring the properties of metal hydrides in order to meet the targets for every day applications [150].

From a technical standpoint, key aspects related to the experimental study of metal hydrides have also been identified. In fact, considerable knowledge was obtained regarding sample preparation, sample handling, hydrogen storage testing and results analysis. As a result, the experimental methodology employed in this work was selected based on proven methods in the literature. Thus, allowing to verify the quality of the experimental implementation through direct comparison of baseline samples against published data. In return, this work will contribute to the literature by providing experimental data on a composition of the Mg-Ni-H system that has yet to be done, $Mg_{72}Ni_{28}$. In addition, the comparison of the acquired experimental results to calculated data obtained through thermodynamic modeling will also support the CALPHAD methodology for metal hydrides investigation.

Chapter 3

Experimental Procedures

The aim of this work is the experimental investigation of the Mg-Ni-H system. It was carried out in three steps: sample preparation, characterization and PCI experiments, as shown below in Figure 3.1. Ni was dissolved into Mg and later crushed into powder with both operations performed under inert atmosphere. Phase identification was carried out using the XRD in the as-cast and hydride state of the sample. Pressure composition isotherms were completed using a Sieverts type apparatus.

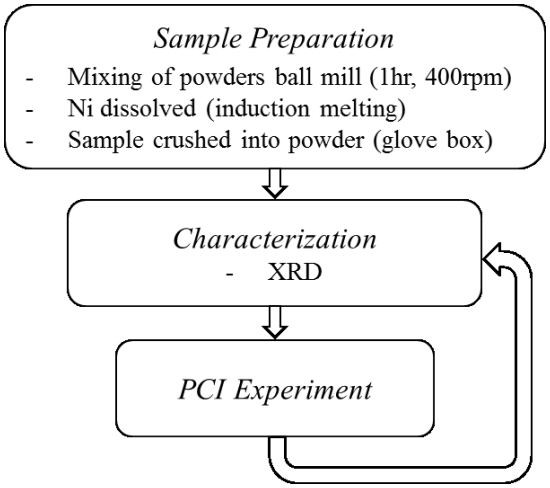

Figure 3.1: Experimental procedure flowchart

3.1 Starting Alloy Preparation

The sample preparation proved to be the most challenging aspect of this work. Several methods were tested for metal alloying such as arc melting, planetary ball milling and Spex high energy ball milling. For the melting technique sample inhomogeneity was the main issue as the melting temperature of the Mg is 650°C and Ni 1455°C. In addition, the use of fairly large pieces (1g) cut from an ingot made it difficult to obtain good mixing

between the two elements. As a result, obtaining homogeneous samples at a desired composition was difficult since even after 5 cycles of crushing and arc melting the button sample remained inhomogeneous. This is due to the high temperature of the arc which caused excessive Mg evaporation and made it impossible to avoid the peritectic reaction in the system that lead to the formation of undesired $MgNi_2$.

Therefore, mechanical alloying techniques were then tested to avoid the melting issues present for the Mg-Ni system. In the case of planetary ball milling, the impact of the balls did not provide enough energy to form the intermetallic compounds even with milling time up to 30 hrs. Therefore, high energy Spex milling was tested at Institut de Recherche sur l'Hydrogène (IRH) in Trois-Rivières. Although we could produce intermetallic compounds by 20 hours of milling and obtain a much finer powder the PCI experiments were unsuccessful due to the presence of contaminants which had detrimental impact on the hydrogen properties of the sample. Consequently, contamination was an issue for both milling techniques as the balls and jar were previously employed for mixing various elements. Although, both the balls and jar were cleaned by milling in alcohol for 0.5 hour, contaminants could be detected in the samples by XRD. As a result, best practices when preparing samples through mechanical alloying consists of always employing a combination of new balls and a new or machined jar for each system to prevent contamination issues.

The technique employed was a variation of the solid state synthesis method used by Zaluska et al. [119] to obtain single phase Mg_2Ni pure samples. They mixed powders of Mg and Ni for 2 hours using Spex ball milling, then annealed the mixture for 15 hours at 400°C. Instead of using both elements in fine powder form typically less than 10

micron for hydrogen storage experiments, larger particle sized Mg powder (149-841 micron) was employed in combination with Ni powder (2.2-3 micron) (Alfa Aesar Mg 99.8%, Ni 99.9%). Once the desired composition of the 2g sample was identified, testing trials showed that an additional 3% (mass) of Mg was necessary to compensate for evaporation losses during synthesis. The powders were mixed under air in a planetary ball mill for 1 hour at 400 rpm. Afterwards, the mixture was melted in the induction furnace under argon environment using a Tantalum crucible. However, since the maximal operating temperature of the furnace is approximately 1050°C the Ni powder was rather dissolved in the liquid Mg. During the melting process, the power of the furnace was slowly increased in order to attain a temperature just above the melting point of Mg. The furnace was held at this point for approximately 3 minutes. Once cooled, the sample was reheated using the same current for a total of five cycles which were sufficient to obtain homogeneous samples of the desired composition as shown in the optical micrograph below in Figure 3.2.

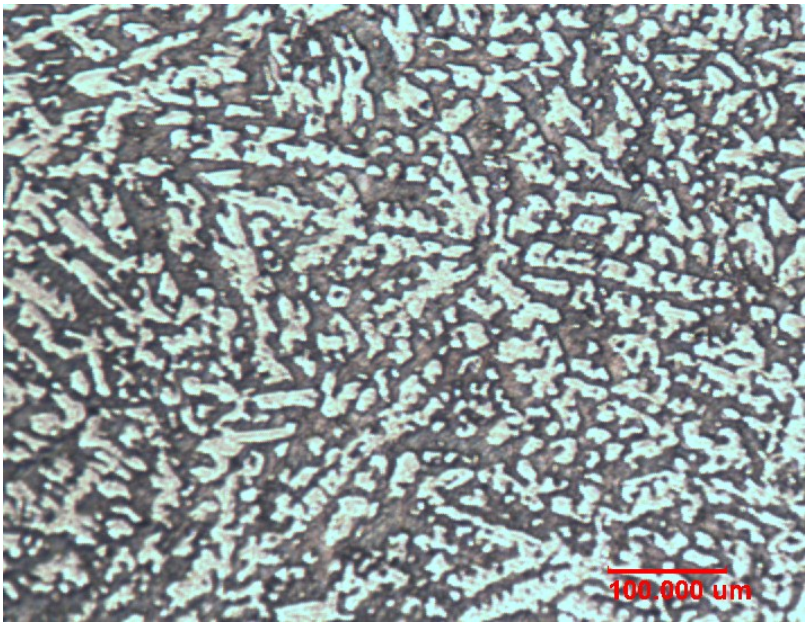

Figure 3.2: Microstructure of as cast sample $Mg_{72}Ni_{28}$

The samples are then crushed into powdered form to maximize surface area for testing. However, powder handling brings up safety concerns such as volatility, self-ignition, contamination and oxidation. Therefore, in order to solve these issues, the samples were manually crushed using a ceramic mortar and pestle in a nitrogen filled glove box in the chemistry lab of Dr. Ottenwaelder in the Loyola campus. While still in the glove box, the powdered sample is weighted and sealed inside the stainless steel test cell using stainless steel metallic gaskets. Although Cu and Ni gaskets are available, it is preferable to use the stainless steel gaskets even if the PCI test is performed below 320°C as some evacuation steps are performed at 400°C.

3.2 Hydrogen Sorption Testing

The equipment used to perform PCI experiments is the Sievert's type PCT-Pro 2000 unit from Setaram Instruments. A picture of the device is shown in Figure 3.3. Once the sample is loaded and the sealed test cell is connected to the volumetric testing apparatus, it is first purged with Helium using the purge system and sample command. The chamber is then degassed for 1 hour at 200°C. Subsequently, volume calibration of the chamber is performed through 4 cycles at the temperature of the desired PCI isotherm using 4 bar of helium. Although precautions were taken to limit oxidation, 3 activation cycles were carried out with a 35 bar pressure for 6 hours followed by 1 hour under vacuum at 400°C.

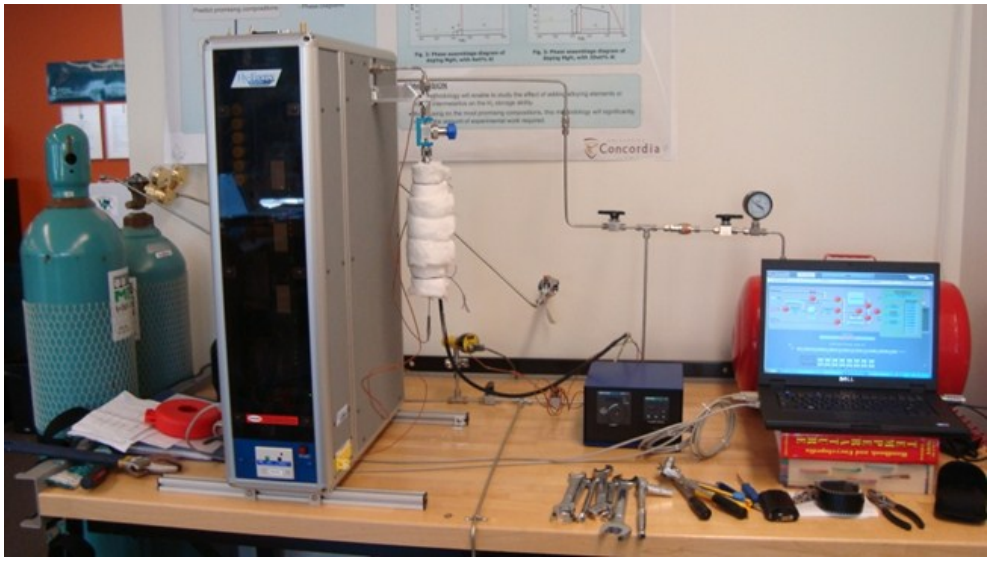

Figure 3.3: PCT-Pro 2000

At this point the sample is ready for PCI testing. Since the PCI experiments take 5-10 hours for Mg alloys, a large amount of data is recorded thus often leading to the LabView software to crash. After discussions with colleagues in the H_2Can network, it became apparent that this issue is common for all PCT-Pro units as well as the in-house made units and is related to the LabView. Therefore, the buffer of the PCT-Pro was cleared by shutting off and restarting the unit and the laptop before each PCI experiment. This allowed to substantially reduce the occurrence of software failure, nonetheless around 1 in 4 experiments would still crash. This issue never arose during desorption PCI tests which typically take less than 1 hour.

The metallic powdered sample then undergoes hydrogen absorption testing at the desired temperature with a pressure step of 0.75 – 1.5 bar and time step of 5-10 mins. For magnesium alloys, the smallest calibrated reservoir volume of 4.58 ml is selected thus offering maximum accuracy. The desorption test is performed with a pressure step of 1

bar, a lower pressure limit of 1 bar and a reservoir volume of 164.3 ml. The lower limit pressure for the desorption experiments is set at 1 bar to allow better comparison between experimental results and storage system for commercial applications. Therefore, in order to extract the maximum amount of hydrogen from the metal before the following absorption cycle, the sample is further desorbed at 400°C for 1 hour. The enclosure heater is always turned on maintaining a reservoir temperature of 26.5 ± 0.4°C.

The experimental error encountered for PCI measurements is ± 0.5 wt. % for hydrogen concentration and ± 10% for the plateau pressure. The error on concentration is the accuracy rating of the unit and it is the typical error associated with Sievert's type testing [100]. Thus this device is unsuitable for performing hydrogen solubility studies that are typically of the order of 0.1 wt. %. However, the experimental error associated with the plateau pressure is due to the discrepancy in sample temperature. As absorption is an exothermic reaction, the temperature of the sample jumps 5-7°C once exposed to hydrogen [101]. However, it is not clearly identified in the literature whether the sample temperature is the initial one or the sample temperature during the reaction with the exothermic contribution. As a result, typically 10 % plateau pressure variations are encountered when comparing experimental results for similar compositions.

3.3 Sample Characterization

The atomic structural evolution and phase transformations were observed through powder diffraction using the Xpert Pro powder Xray diffractometer from PANanalytical. Peak identification and Rietveld analysis were performed using X'Pert HighScore Plus software also from PANalytical in combination with Pearson's crystal database [151].

The XRD was operated under CuKα radiation at 45kV and 40mA and the XRD spectrum was collected from 10 to 80º 2θ with a 0.02º step size.

All diffraction patterns were obtained with samples exposed in air for the entire duration of the programmed scan. A portion of the metallic powder sample was used for XRD analysis in the as-cast condition i.e., before any hydrogen sorption testing. Following the hydrogen absorption experiment, the sample is cooled to room temperature under 20 bar hydrogen pressure thus remaining in the hydrided state, and then XRD is performed. It is important to note that satisfactory XRD results for the MgH_2 and Mg_2NiH_4 hydride phases could be obtained mainly due to the fact that these hydrides are stable in air long enough to capture the diffraction patterns. However, this is not the case for all hydrides and care should be taken to perform XRD of hydrides under inert environment to prevent sample degradation. In fact, after hours of air exposure, the color of the powder changed from light grey to white as even these more stable hydrides are still sensitive to oxygen and humidity.

Chapter 4

Experimental Results and Discussion

In this chapter, the PCI experiments of two samples in the Mg-Ni-H system are presented, $Mg_{67}Ni_{33}$, $Mg_{72}Ni_{28}$. At first, the experimental data are validated by literature experiments then they are compared with calculated results from thermodynamic modeling. PCI results from the $Mg_{67}Ni_{33}$ sample were found to be in good agreement with published data for the same composition. In addition, the XRD pattern for that composition and its Van't Hoff plot also corresponded to published results. Furthermore, the catalytic role of Ni was highlighted by the PCI and Van't Hoff results obtained for the $Mg_{72}Ni_{28}$ sample. The PCI data from this composition was found to be in good agreement with the predicted values from the thermodynamic model.

Only absorption experiments are shown in the first section as the literature predominantly depicts absorption curves. However, since the equilibrium lies halfway between the absorption and desorption, both absorption and desorption curves are included to allow comparison with the calculated equilibrium results from the thermodynamic model.

4.1 Preliminary Testing

At the start of the project, a commercial unit from Setaram Instruments was purchased. The apparatus was installed and baseline test were successfully completed using a pure Palladium sample. The results obtained matched the standards provided by the company at 180°C using the same unit and are in good agreement with literature data as shown in Figure 4.1.

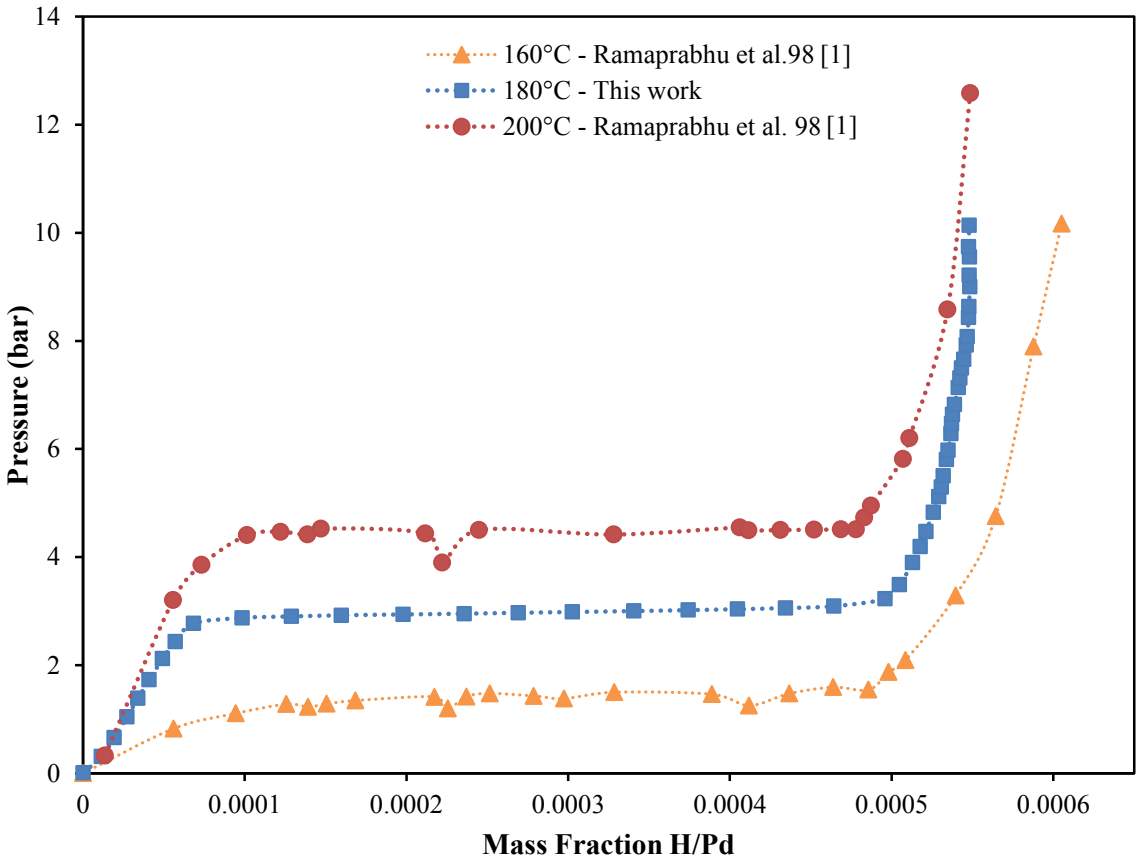

Figure 4.1: PCI absorption pure Pd 180°C compared to literature

Experimental investigation of the hydrogen sorption properties of metal hydrides is long and tedious. In fact, it took well over 12 months and 70 test cycles to establish adequate experimental procedures in terms of sample preparation and testing parameters.

The process of activation is not quite clearly defined and systems behave rather differently. Therefore, the initial activation cycles for a new sample were performed as PCI experiments, where data is collected. Although this makes activation longer, it is the most direct way to monitor the state of the sample. Pure Mg and MgNi samples absorbed H_2 during the first cycle but were fully activated after 3 cycles. In comparison, samples in the MgCuY system did not store any hydrogen at first and required 10 cycles for complete activation, as shown in Figure 4.2. In contrast, samples of the Mg-Ca system

could never reach full activation even after more than 15 sorption cycles. Furthermore, only one experimental source could be found on the system [152], again portraying the difficulties surrounding PCI experiments and especially when dealing with oxygen sensitive elements.

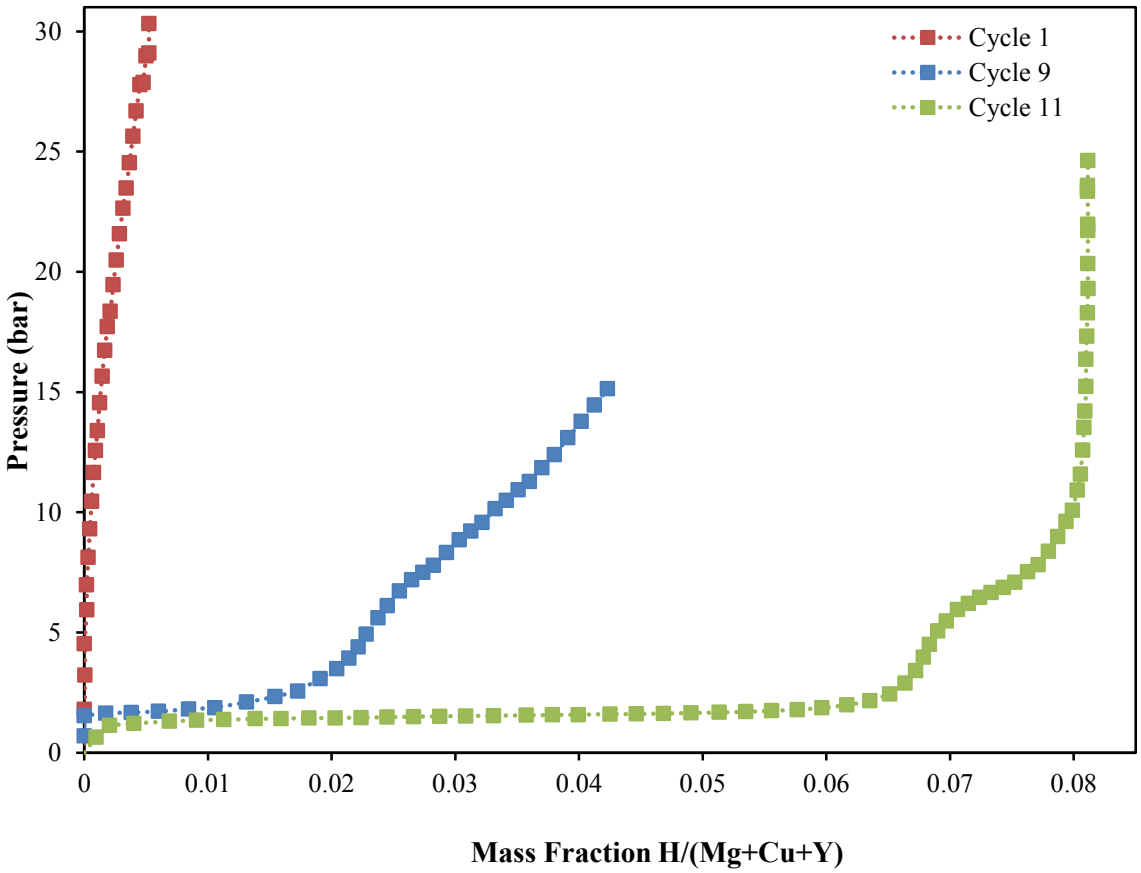

Figure 4.2: PCI activation cycles $Mg_{64.3}Cu_{15.7}Y_{20}$ at 300°C

4.2 Mg-Ni-H Experimental Results

The $Mg_{67}Ni_{33}$ sample was chosen due to the considerable amount of experimental data reported for that composition thus making it ideal for thorough comparison. As for the $Mg_{72}Ni_{28}$ sample, no experimental data has been reported for that composition. The absorption PCI data presented contains no kinetic data as the current configuration of our PCT-Pro 2000 unit did not include the optional time-based measurements. However, this

did not limit the scope of this work as the information needed for phase diagram development is based on equilibrium data which are provided by PCI experiments.

4.2.1. $Mg_{67}Ni_{33}$ Experimental Results

The $Mg_{67}Ni_{33}$ composition was successfully prepared. As shown in Figure 4.3, XRD results reveal sharp crystalline diffraction peaks that correspond to the diffraction pattern of the Mg_2Ni intermetallic phase. No Mg or $MgNi_2$ peaks could be observed thus confirming the homogeneity of the sample. In addition, no oxide peaks are present.

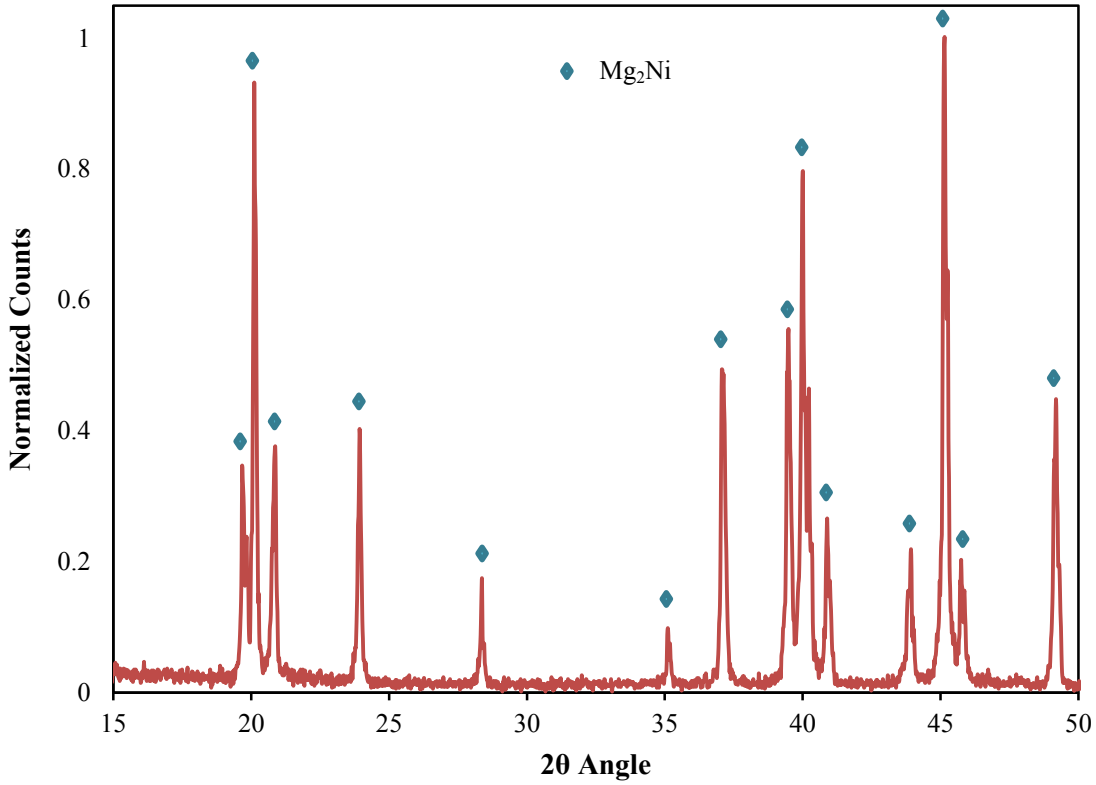

Figure 4.3: XRD as cast $Mg_{67}Ni_{33}$

The absorption PCI results for the $Mg_{67}Ni_{33}$ sample at 300°C is presented in Figure 4.4. The obtained results are compared with literature data from 3 sources Zaluski 1995 [87] , Reilly et al. 1968 [143], and Buchner et al. 1978 [153]. The hydrogen absorption reaction captured contains a single plateau which corresponds to the formation

of Mg_2NiH_4 phase. It can be seen, that the results obtained are in good agreement with literature data. The obtained plateau pressure is 3.51 bar with a maximum storage of 3.2 wt. %. In fact, both the maximum hydrogen concentration and the plateau pressure concord with the data from Zaluski. The other two older sources were included to support solely the plateau pressure, since only a partial portion of the absorption curve was presented in both. However, the low pressure solid solution data obtained is larger than all three references. Yet, the current results are well within the experimental error.

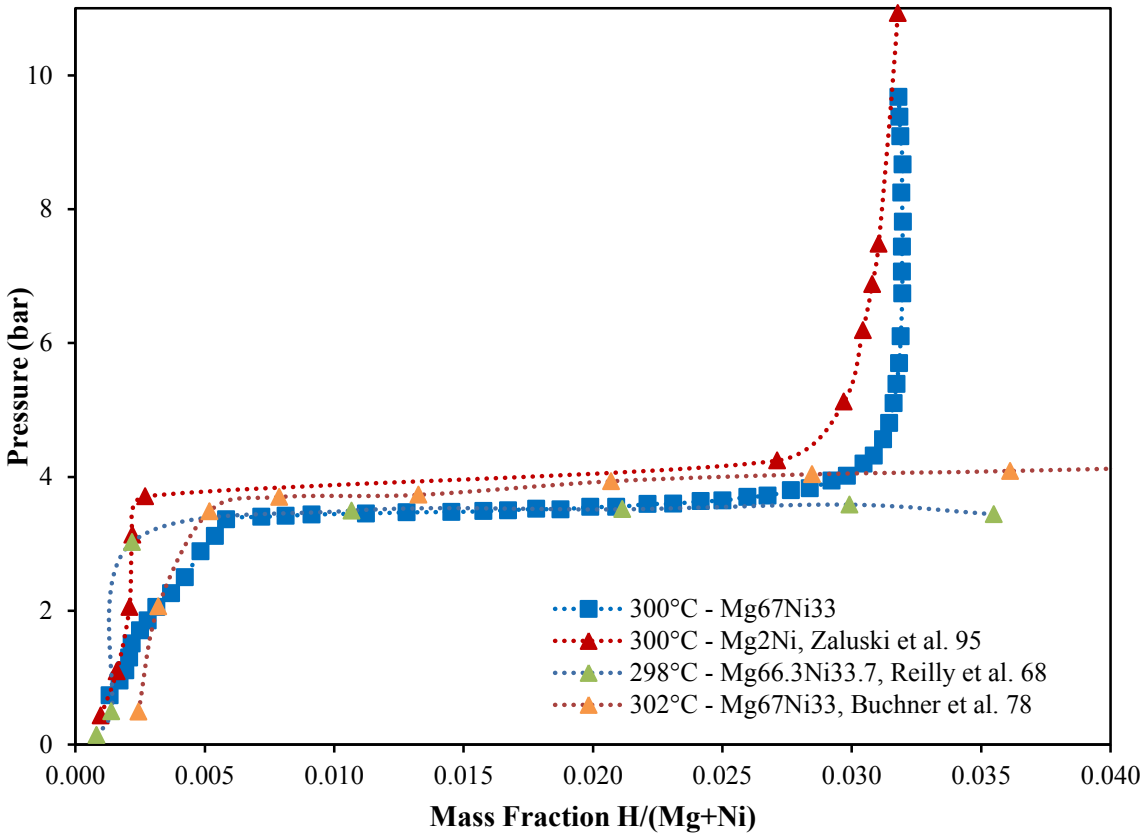

Figure 4.4: PCI absorption $Mg_{67}Ni_{33}$ at 300°C compared to literature

A set of PCI tests was performed for the $Mg_{67}Ni_{33}$ sample and the results are shown in Figure 4.5. This plot of absorption PCI at three different temperatures provides the information necessary for phase diagram development. The summary of the

information concerning the plateaus can be found in Table 4.1. The low pressure solid solution storage is similar in all 3 tests at about 0.6 % wt. In addition, it can be observed that the maximum hydrogen concentration decreases with increasing temperature. In effect, 3.2 % is stored at 300°C which drops to 3.0 % wt. at 325°C and 2.6 % wt. is absorbed at 350°C. This aspect describes the evolution of the phase boundary between ($Mg_2Ni+Mg_2NiH_4+H_2$) and ($Mg_2NiH_4+H_2$).

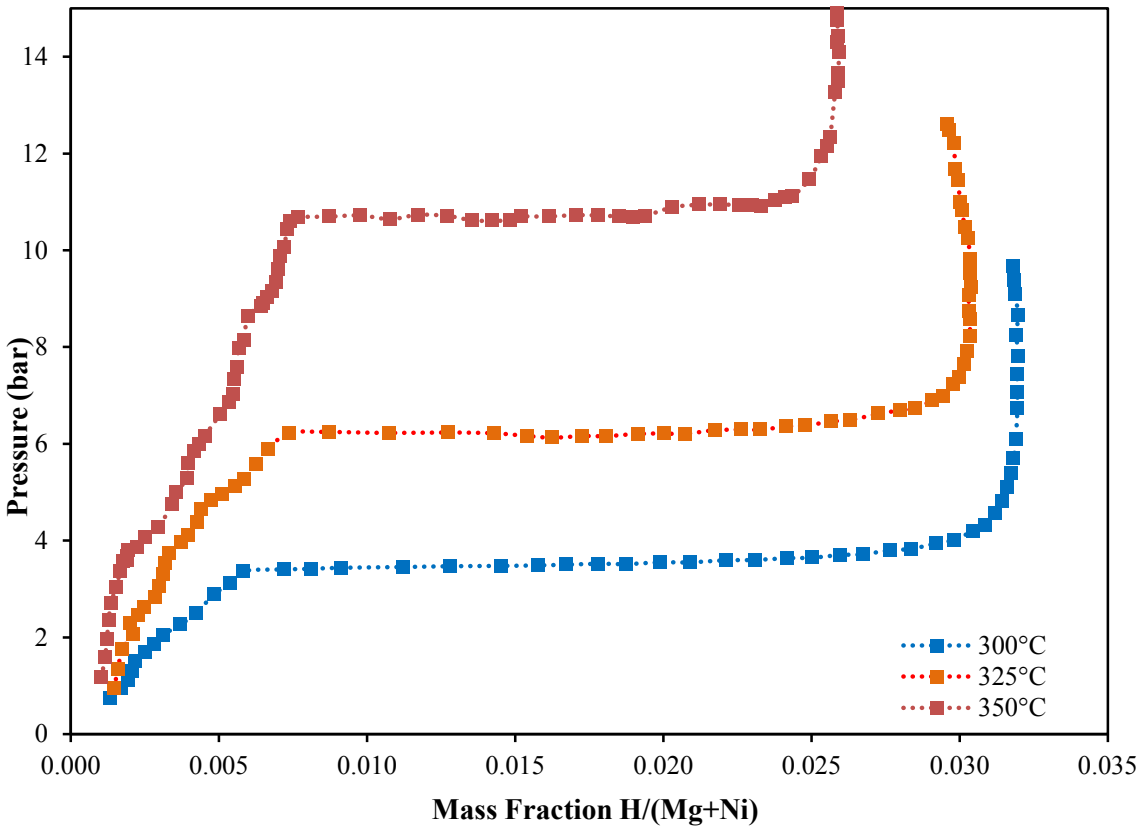

Figure 4.5: PCI absorption $Mg_{67}Ni_{33}$ at 300, 325, 350°C

Table 4.1: Absorption plateau pressures of $Mg_{67}Ni_{33}$

Temperature (°C)	Phase	Pressure (bar)
300	Mg_2NiH_4	3.41
325		6.21
350		10.70

In addition to observing a plateau during PCI testing of Mg_2Ni pure sample, phase identification of the XRD pattern of the powder after the absorption PCI also confirmed the presence of Mg_2NiH_4, as shown in Figure 4.6. Furthermore, substantial peak broadening can also be observed as the activation cycles severely broke down the grains thus refining the average crystallite size of the sample. Nonetheless, all the high intensity diffraction peaks observed could be linked to the diffraction pattern of the Mg_2NiH_4 ternary hydride. However, the few unidentified peaks can be attributed to the allotropic transformation of Mg_2NiH_4 at 235°C [154, 155] which took place during sample cooling to room temperature and were intentionally left out.

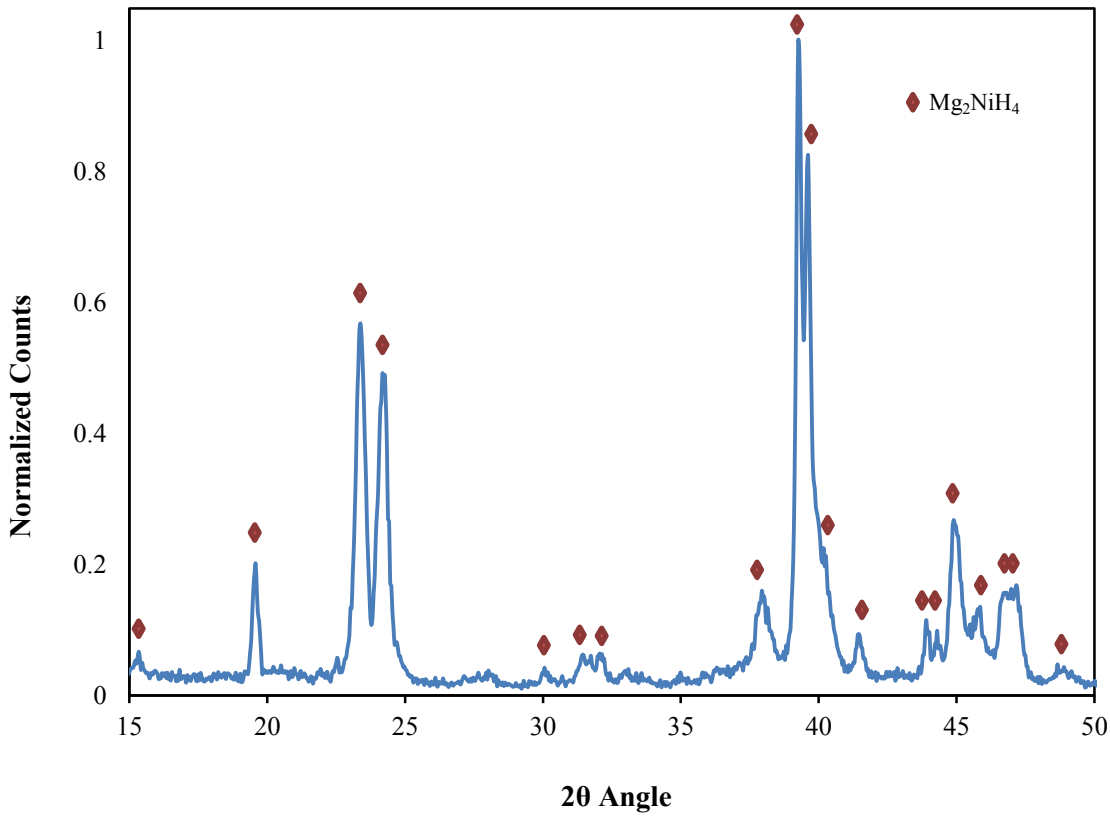

Figure 4.6: XRD hydrided $Mg_{67}Ni_{33}$

From the three PCI experiments in Figure 4.5 we can obtain the Van't Hoff plot for the Mg_2NiH_4 hydride formation, shown below in Figure 4.7. The experimental enthalpy of formation of Mg_2NiH_4 calculated from the absorption PCI data is $\Delta H = -67.8 \pm 5.5$ kJ/mol H_2, thus in close agreement with the -62 to -64 kJ/mol H_2 range reported in the literature [143, 156]. The margin of error results from uncertainty with respect to the sample temperature of ± 2.0°C.

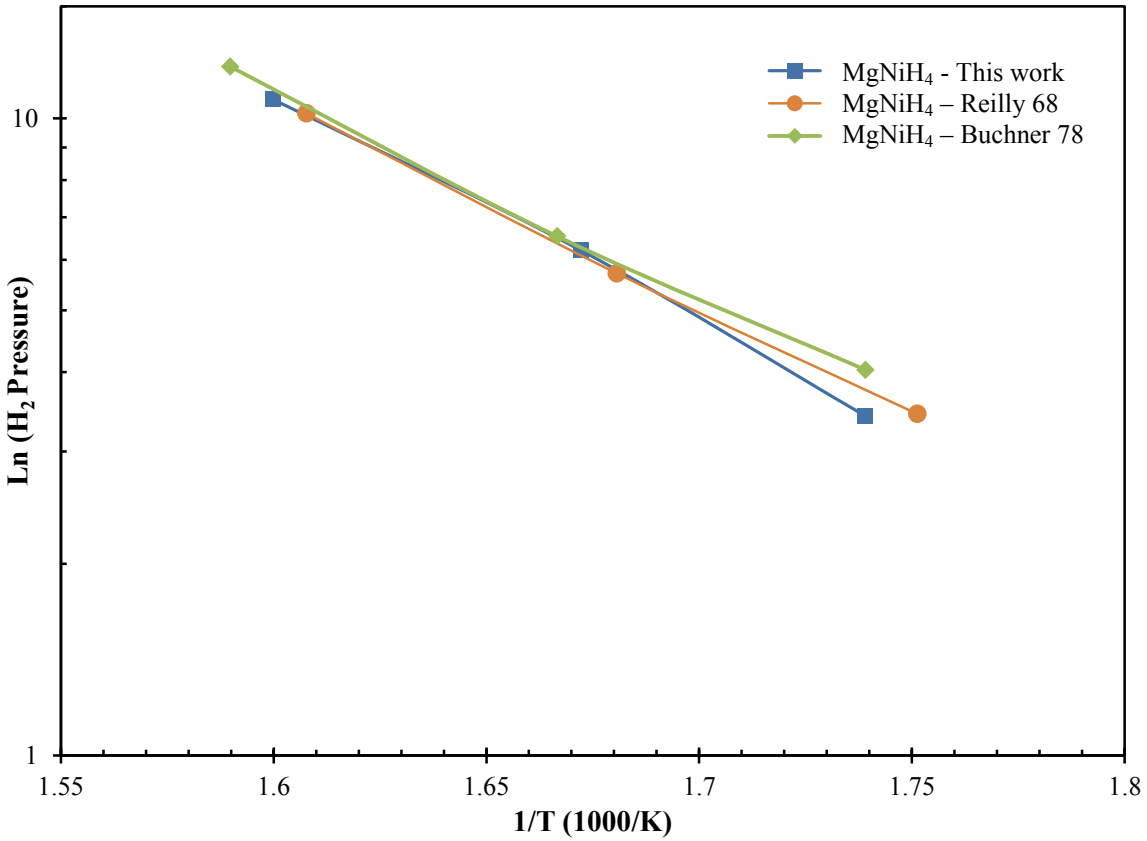

Figure 4.7: Van't Hoff plot Mg_2NiH_4 in $Mg_{67}Ni_{33}$ compared to literature

4.2.2. $Mg_{72}Ni_{28}$ Experimental Results

The XRD results of the $Mg_{72}Ni_{28}$ composition confirmed that the sample was successfully prepared, as shown in Figure 4.8. In fact, the sharp diffraction peaks of both the Mg_2Ni and the Mg were positively identified as the two phases present in the sample. Even with the numerous peaks present, no peak overlap was encountered.

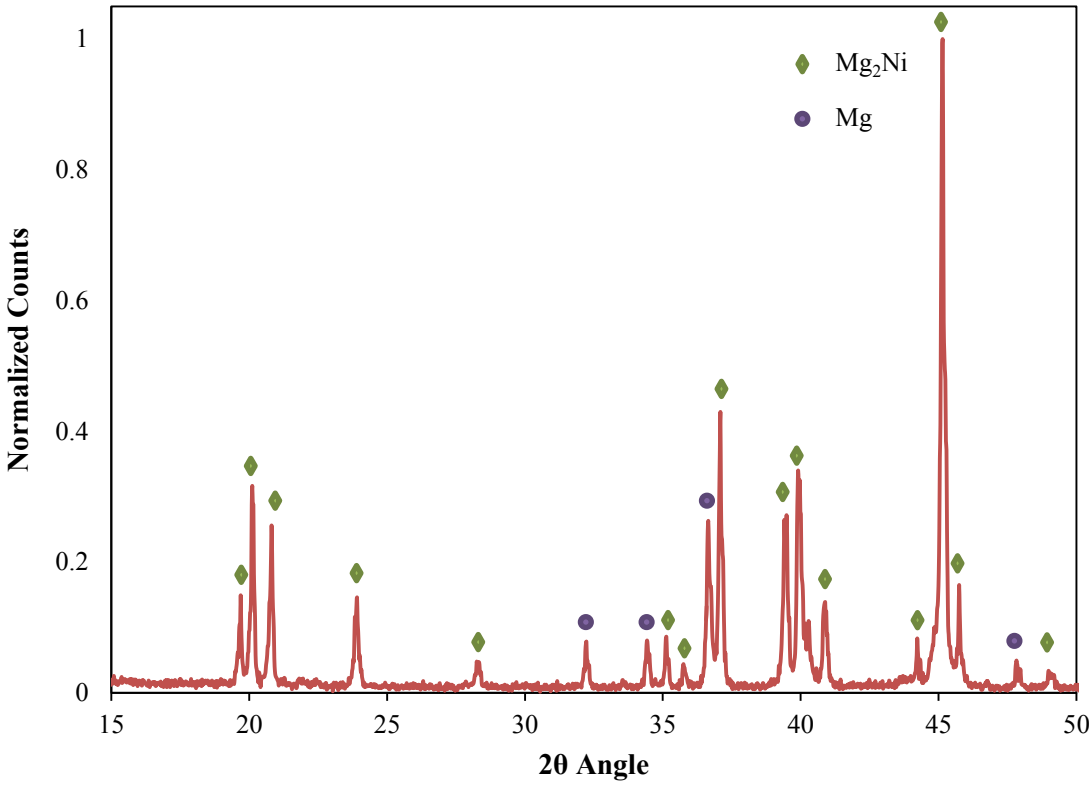

Figure 4.8: XRD as cast $Mg_{72}Ni_{28}$

The results from the PCI absorption tests of $Mg_{72}Ni_{28}$ are shown in Figure 4.9. As anticipated, two plateaus can be seen in the absorption PCI plots. The first one consists of the formation of the MgH_2 and the second the formation of Mg_2NiH_4. The plateau pressures for the different hydrides are summarized below in Table 4.2. It can be seen that the obtained plateau pressures and the hydrogen concentrations are in good accord and provide the correct phase boundary trends. Approximately 1 wt. % of hydrogen is stored by the MgH_2 for all three experiments. As for the $MgNiH_4$ hydride phase, it stores less hydrogen as the temperature increases again depicting the same phase boundary trend as seen in the PCI of the $Mg_{67}Ni_{33}$ sample. The stored hydrogen is 2.5 wt. % at 300°C, 2.4 wt. % at 325°C and 2.3 wt. % at 350°C, as identified by the arrowed lines in Figure 4.9.

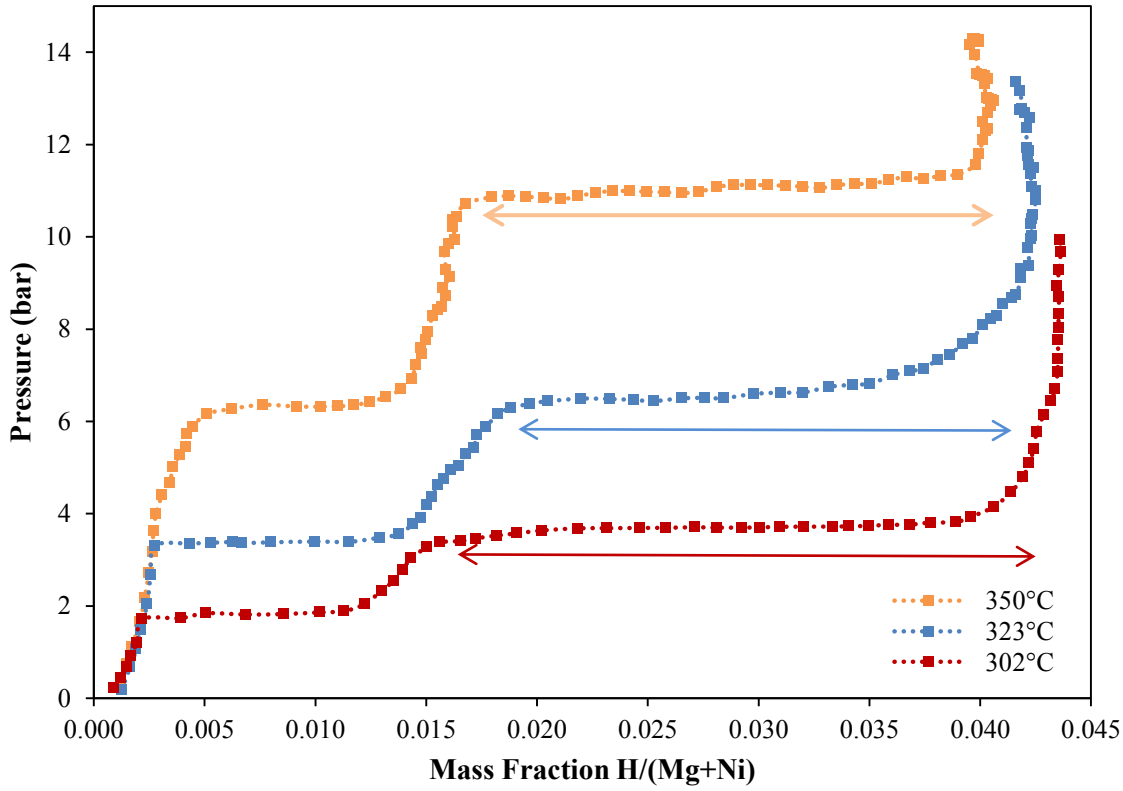

Figure 4.9: PCI absorption $Mg_{72}Ni_{28}$ at 300, 325, 350°C

Table 4.2: Absorption plateau pressures of $Mg_{72}Ni_{28}$

Temperature (°C)	Phase	Pressure (bar)
300	Mg_2NiH_4	3.70
	MgH_2	1.82
325	Mg_2NiH_4	6.50
	MgH_2	3.38
350	Mg_2NiH_4	10.95
	MgH_2	6.32

Furthermore, the plateau pressure of MgH_2 is also in good agreement with the literature results for pure Mg samples [106]. This aspect confirms the catalytic role of Ni as the thermodynamic properties of the Mg → MgH_2 reaction remain unchanged with the

presence of Ni. As only equilibrium measurements were performed, it is therefore expected that the Mg plateau be unchanged even in a sample rich of the Mg_2Ni phase. On the other hand, the plateau pressure for Mg_2NiH_4 remained unchanged by the presence of Mg phase in the sample as Mg does not play a role in the formation reaction of Mg_2NiH_4. This can be seen by comparing the plateau pressure for the Mg_2NiH_4 in Figure 4.5 and Figure 4.9.

The formation of the two hydrides was also confirmed by XRD result for the $Mg_{72}Ni_{28}$ as shown below in Figure 4.10. Again, peak broadening was observed along with some unresolved low intensity peaks which are again related to the Mg_2NiH_4 allotropic transformation.

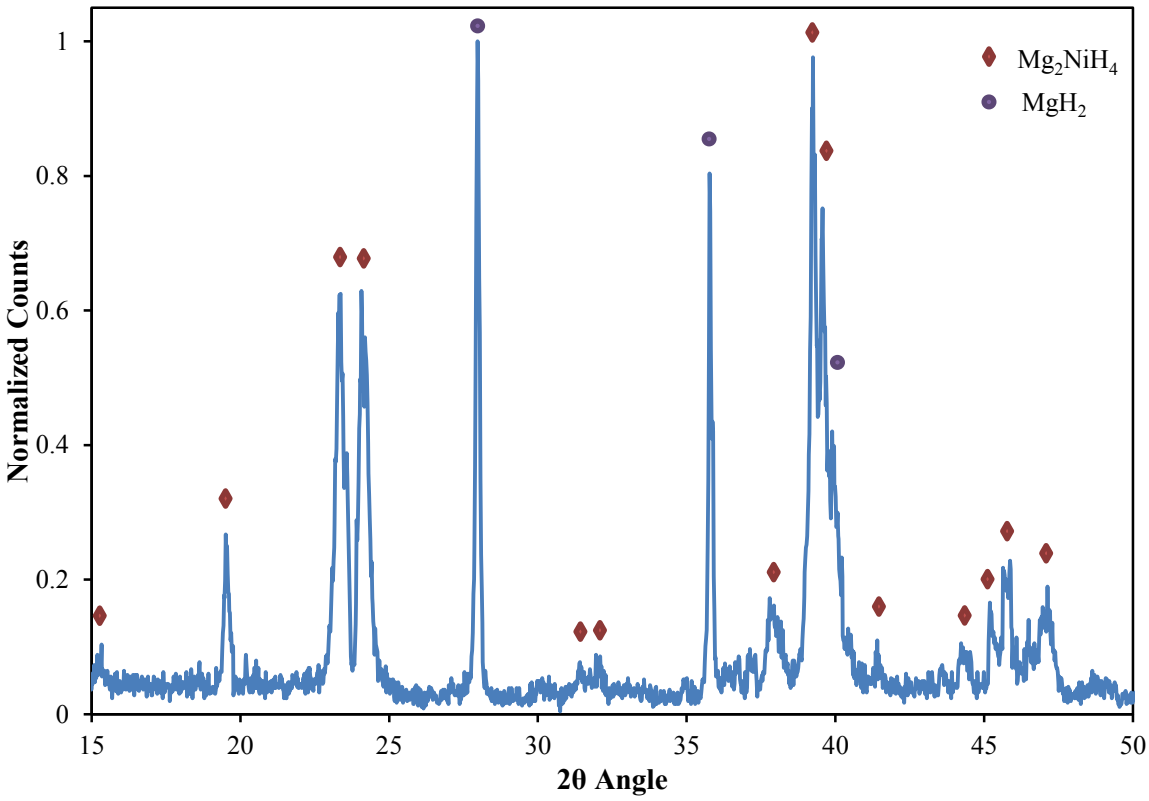

Figure 4.10: XRD hydrided $Mg_{72}Ni_{28}$

As shown in Figure 4.11, the Van't Hoff plot from the two hydrides present in the $Mg_{72}Ni_{28}$ sample was drawn using the PCI absorption results discussed earlier. The plot show good agreement between the obtained data and the published results. The experimental enthalpy of formation of Mg_2NiH_4 and MgH_2 calculated from the absorption PCI data are respectively $\Delta H = -64.4 \pm 4.8$ kJ/mol H_2 and $\Delta H = -74.0 \pm 5.5$ kJ/mol H_2. Once more, there is good agreement with published thermodynamic data on the two hydrides, -62 to -64 kJ/mol for Mg_2NiH_4 [143] and -72 to -75 kJ/mol H_2 for MgH_2 [157]. In addition, these thermodynamic results confirm yet again the catalytic role of Ni as the enthalpy of Mg is the same as the one obtained from pure Mg PCI experiments.

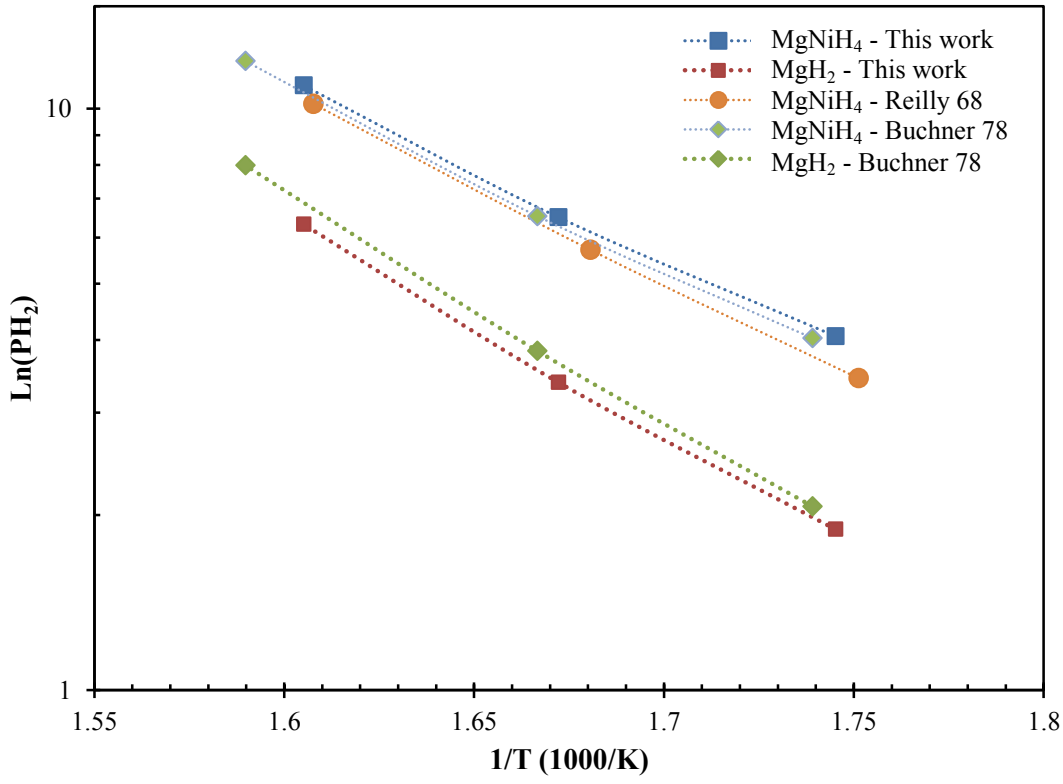

Figure 4.11: Van't Hoff plot Mg_2NiH_4 and MgH_2 in $Mg_{72}Ni_{28}$ compared to literature

4.3 Mg-Ni-H Modeling Results

The thermodynamic modeling of the Mg-Ni-H system is compared with the experimental results in this section. The modeling results shown were obtained from the multicomponent database prepared using the CALPHAD method with the FactSage software prepared by Saida Abdessameud [158]. The model not only provides thermodynamic information on the system it can also predict the hydrogen capacity of any compositions in the system, the phase formation and transformations during hydrogen sorption and the heat of reaction. These aspects of thermodynamic modeling allow to substantially reduce the amount of experimental work needed to obtain a complete understanding of a system.

Five different types of stable phases have been described in the Mg-Ni-H system. The first type is the gas phase used for H_2, Mg and Ni gases which are treated as an ideal solution. The second type is the ternary solid solution phases, FCC-(Ni) and HCP-(Mg), which are described by two-sublattice models where Mg and Ni substitute for each other in the first sublattice and hydrogen atoms and vacant interstitial sites in the second one. They are represented by the models: $(Mg, Ni)_1(H,Va)_1$ for FCC-(Ni) and $(Mg, Ni)_2(H,Va)_1$ for HCP-Mg. The third type is the solid solution of γ (Mg_2Ni) with hydrogen that has a composition range of Mg_2NiH_x ($x \leq 0.3$) which is described by the $(Mg)_2(Ni)(H,Va)_1$ sublattice model. The fourth type is the liquid phase modeled using the modified quasichemical model. At last, the fifth type is the intermetallic compound used to describe MgH_2 and Mg_2NiH_4 which are considered stoichiometric.

Two key comparison aspects between experimental results and the theoretical results from the model are the plateau pressure of phase transformations and the storage capacity

of hydride phases. A summary of the experimental and theoretical equilibrium plateau pressure is given in Table 4.3, where the midpoint pressure is the average of the absorption and desorption pressures.

Table 4.3: Plateau pressure for $Mg_{67}Ni_{33}$ and $Mg_{72}Ni_{28}$ at 325°C (in bar)

Sample	Phase	Absorption	Desorption	Midpoint	Model
$Mg_{67}Ni_{33}$	Mg_2NiH_4	6.21	3.86	5.04	4.53
$Mg_{72}Ni_{28}$	Mg_2NiH_4	6.50	3.94	5.22	4.68
	MgH_2	3.38	2.33	2.86	2.76

As shown in Table 4.3, there is good agreement between the plateau pressures of the experimental results and those from the model. In fact, for all three cases the predicted plateau pressure from the model lies in between the experimental absorption and desorption pressures. Nonetheless, it can also be observed that the disparity between the midpoint pressure and the model pressure is 10% for the Mg_2NiH_4 and 4% for the MgH_2, thus well within the experimental error associated with PCI measurements. Therefore, the model is more accurate in predicting the MgH_2 transformation than the Mg_2NiH_4 transformation. Furthermore, optimization of the modeling parameters could improve the results for the ternary hydride transformation.

The comparison of the experimental PCI results to the calculated data from the model is respectively shown for the $Mg_{67}Ni_{33}$ and $Mg_{72}Ni_{28}$ sample in the Figure 4.12 and Figure 4.13. It can be seen by the arrowed line on the figures that the experimental amount of stored and released hydrogen for all the plateaus is lower than the theoretical amount given by the model. This is related to the fact that it is impossible to fill all the available sites in the sample with hydrogen atoms in practice. In fact, for experimental samples the energy level of the available sites for hydrogen atoms follows a distribution

where some sites have an energy level too high to be filled during absorption. In addition, the hydrogen absorption reaction cannot reach the entire volume of the powder particles due to slow diffusion. As a result, some sites remain empty thus reducing the total amount of stored H_2. This is also true in the case of desorption, some hydrogen atoms have high bonding energy and cannot be released during desorption. Although optimization of the powder processing technique and processing parameters help in maximizing the hydrogen capacity of a sample, the theoretical plateau length is always greater than the experimental amount of stored or released hydrogen.

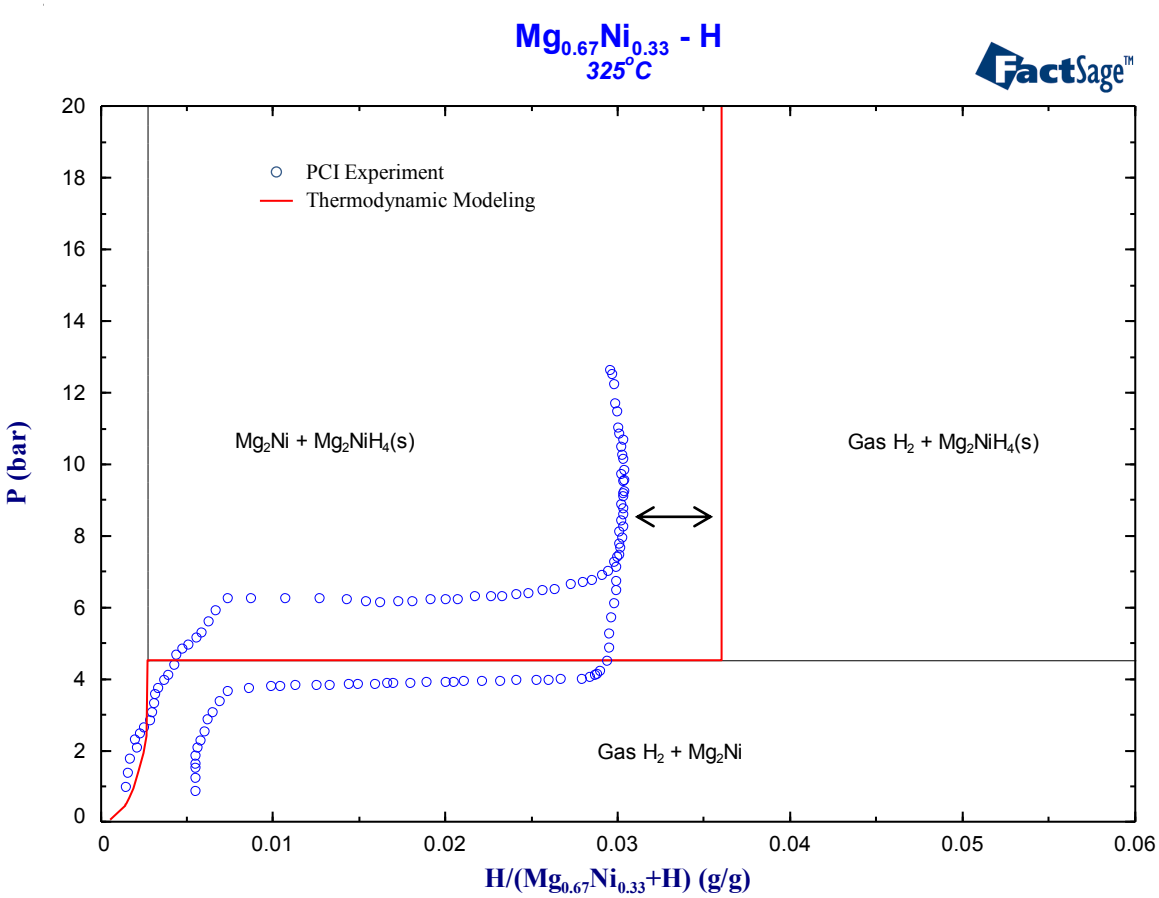

Figure 4.12: Calculated PCI of $Mg_{67}Ni_{33}$ at 325°C [158]

The plateau pressures obtained experimentally for the hydride transformation concord with the theoretical data. Indeed, the plateau predicted by the model falls in

between the absorption and desorption curves for both the $Mg_{67}Ni_{33}$ and the $Mg_{72}Ni_{28}$ samples, thus respecting the thermodynamic concepts for the equilibrium reaction. Furthermore, the calculated PCI for the $Mg_{72}Ni_{28}$ sample (Figure 4.13) shows that the model is also accurate in the prediction of the ternary hydride formation even when another hydride phase is the present.

With a lower limit of 1 bar during desorption, only 0.4% of hydrogen remained in the sample for both compositions. Therefore, this system has good reversibility since the $Mg_{67}Ni_{33}$ and $Mg_{72}Ni_{28}$ respectively released 87% and 91% of their hydrogen capacity without being exposed to vacuum. The hysteresis is around 2 bar for the Mg_2NiH_4 transformation while it is 1 bar for the MgH_2 plateau. The experimental enthalpy obtained from the desorption reaction of the Mg_2NiH_4 phase is 75.5 ± 5.5 kJ/mol for the $Mg_{67}Ni_{33}$ sample. As for the $Mg_{72}Ni_{28}$ sample, the experimental enthalpy obtained from the desorption reaction of the Mg_2NiH_4 phase was 73.0 ± 3.1 kJ/mol and 82.1 ± 5.5 kJ/mol for the MgH_2 phase.

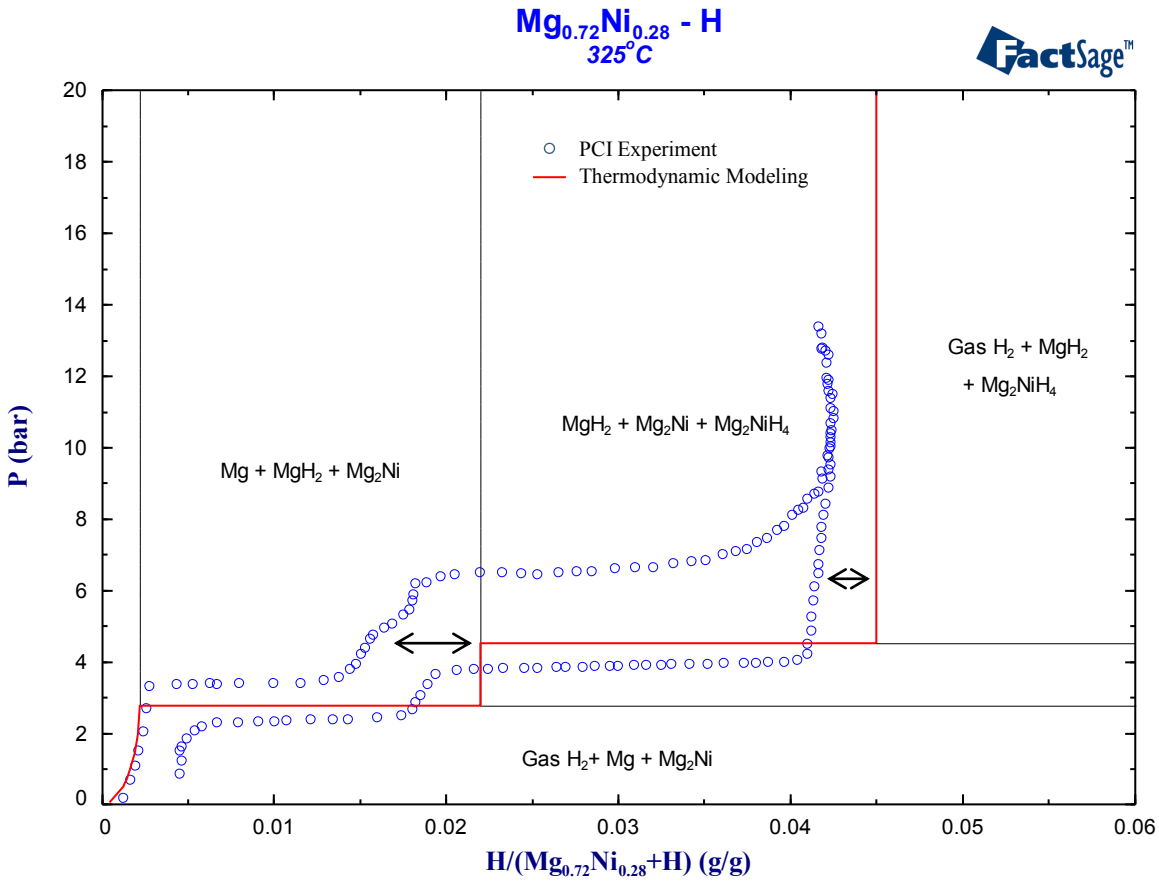

Figure 4.13: Calculated PCI of $Mg_{72}Ni_{28}$ at 325°C [158]

When analyzing the thermodynamic parameters of the hydride formation and decomposition for the two samples, we obtain a complete understanding of the reactions at hand. The experimental enthalpies for the hydride reactions in both samples are shown in Table 4.4. At first glance, it can be seen that although there is good agreement between the experimental data and the values reported in the literature, the desorption enthalpy is always higher than the absorption enthalpy. This can be attributed to the lower plateau pressure of the desorption process which relates to higher stability since the PCI testing temperature is the same as for the absorption test. Again, the error associated with desorption enthalpy is related to the endothermic behavior of the reaction which lowers the sample temperature. Therefore the sample temperature should be increased by 2-3° to

compensate for the endothermic effect which result in lowering the desorption enthalpy of the sample.

Table 4.4: Enthalpy for the $Mg_{67}Ni_{33}$ and $Mg_{72}Ni_{28}$ at 325°C

Sample	Reaction	Experimental ΔH (kJ/mol)	Calculated ΔH (kJ/mol) [158]	Reported ΔH (kJ/mol) [159]
$Mg_{67}Ni_{33}$	Mg_2NiH_4 Absorption	-67.8		-
	Mg_2NiH_4 Desorption	-75.5		-
	Mg_2NiH_4 Average	-71.7 ± 5.5	- 66.4	-64.5
$Mg_{72}Ni_{28}$	Mg_2NiH_4 Absorption	-64.4		-
	Mg_2NiH_4 Desorption	-73.0		-
	Mg_2NiH_4 Average	-68.7 ± 5.5	-66.4	-64.5
	MgH_2 Absorption	-74.0		-
	MgH_2 Desorption	-82.1		-
	MgH_2 Average	-79.8 ± 5.5	-78.8	-77.4

The calculated PCI results discussed above play a crucial role in the validation of the thermodynamic model. In fact, they provide confidence in the calculated phase diagram. The ternary Mg-Ni-H isothermal phase diagram that was calculated at 325°C using thermodynamic modeling is presented Figure 4.14. In this figure, the relation between the experimental PCI plots from the previous section and the ternary phase diagram for the Mg-Ni-H system can be observed. In fact, the PCI curves appear as straight lines, where the blue represents the $Mg_{72}Ni_{28}$ sample while the red is the $Mg_{67}Ni_{33}$ sample. It can be seen that the equilibrium plateaus for the hydride transformation appear here as regions on the phase diagram. As such, the PCI experiments serve as building blocks for the construction of the phase diagram.

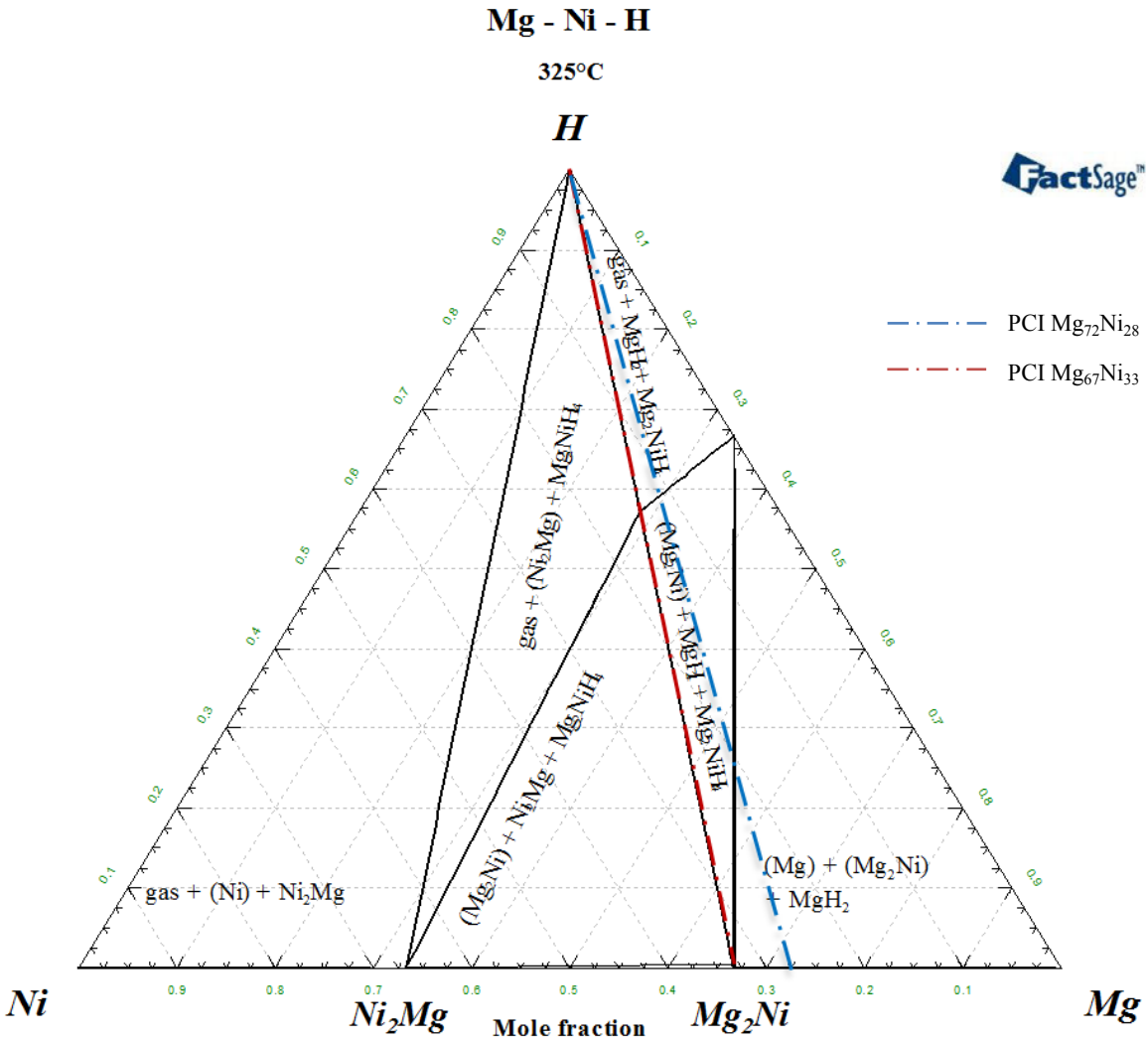

Figure 4.14: Calculated isothermal section of Mg-Ni-H at 325°C [158]

Chapter 5

Summary and Future Work

Absorption and desorption PCI experiments were successfully carried out for two compositions in the Mg-Ni-H system, namely, $Mg_{67}Ni_{33}$ and $Mg_{72}Ni_{28}$. In addition, several other samples have been tested for calibration and validation purposes such as Pd, MgCuY and MgCa. The difficulties encountered with sample preparation were resolved and homogeneous and oxidation free powder samples could be produced.

The collected experimental PCI results on the Mg-Ni-H system were shown to be in good agreement with literature data. In fact, XRD patterns, PCI data and Van't Hoff plots were in good accordance with published data for the $Mg_{67}Ni_{33}$ composition. In addition, new data points for the system were obtained through the PCI testing of the $Mg_{72}Ni_{28}$ sample. Furthermore, the results for the $Mg_{72}Ni_{28}$ composition were consistent with the calculated theoretical PCI data provided by thermodynamic modeling. Consequently, the effectiveness of the novel metal hydride investigation methodology, consisting of key samples combined with thermodynamic modeling, was validated. In fact, the thermodynamic representation of the $Mg_{(100-x)}Ni_{(x)}$ ($0 \leq x \leq 33$) composition range of the system was obtained through 2 key samples.

In addition, as this project was the first work on hydrogen storage performed in our group, the comprehensive review of the literature on hydrogen storage completed and the experimental procedure developed are key contributions for upcoming students working on metal hydrides.

For future experimental investigation of metal hydride systems, it is recommended to use high energy Spex ball milling for sample preparation as it provides a fine powder sample and introduces defects that accelerate the activation process. More importantly, an argon filled glove box should be used for sample manipulation as oxidation has severe detrimental impact on the PCI testing of the majority metal hydride samples. In addition, argon is also more suitable for milling environment as nitrogen can react with the metal hydride powders during extended milling.

In terms of PCI testing, at activation cycles have to be carried out on the metallic sample prior to collecting data. However, the desorption lower pressure limit, the time step and pressure step should be selected carefully as these parameters have considerable impact on the sorption properties of the sample. For instance, $LiBH_4$ loses its hydrogen storage ability when exposed to a pressure below 1 bar, due to a decomposition reaction. A thorough literature review can provide insight on testing parameters for a number systems. On the other hand, for new systems, testing parameters can be approximated by performing a quick hydrogen sorption experiment without reaching complete equilibrium conditions.

A kinetic study of the investigated metal hydride systems could be performed to assess the usefulness of that system for everyday life applications and to better understand the role of certain alloying elements. Nonetheless, PCI experiments provide more insight on the thermodynamic properties of the sample under study. In order to contribute to the understanding of the systems that include Boron, Hydrogen, Lithium, Magnesium and Nickel, future research efforts ought to be aimed towards samples composed of metallic and complex hydrides. Furthermore, using the key experiments

combined with thermodynamic modeling method allows for rapid investigation of these composite materials which can offer good reversibility with large volumetric and gravimetric capacity [120, 136, 150].

References

1. S. Ramaprabhu, N. Rajalakshmi, and A. Weiss: Design and development of hydrogen absorption/desorption high pressure apparatus based on the pressure reduction method. *International Journal of Hydrogen Energy*, Vol. 23, No. 9, 1998, pp. 797-801.

2. M.K. Hubbert: Energy Ressources, 1962, U.S. National Academy of Sciences: Washington D.C. pp. 96.

3. G. Principi, F. Agresti, A. Maddalena, and S. Lo Russo: The problem of solid state hydrogen storage. *Energy*, Vol. 34, No. 12, 2009, pp. 2087-2091.

4. M. Korpås and C.J. Greiner: Opportunities for hydrogen production in connection with wind power in weak grids. *Renewable Energy*, Vol. 33, No. 6, 2008, pp. 1199-1208.

5. G. Nolan: Applications For Fuel Cells, *Silicon Chip*, No. 166, 2002.

6. M. Alsheyab, J.-Q. Jiang, and C. Stanford: Risk assessment of hydrogen gas production in the laboratory scale electrochemical generation of ferrate(VI). *Journal of Chemical Health and Safety*, Vol. 15, No. 5, 2008, pp. 16-20.

7. A. Züttel, A. Borgschulte, and L. Schlapbach: *Hydrogen as a Future Energy Carrier*, 1 ed, Wiley-VCH Verlag GmbH & Co. KGaA, 2008.

8. S. McWhorter, C. Read, G. Ordaz, and N. Stetson: Materials-based hydrogen storage: Attributes for near-term, early market PEM fuel cells. *Current Opinion in Solid State and Materials Science*, Vol. 15, No. 2, 2011, pp. 29-38.

9. U.S Department Of Energy: Multi-Year Research, Development and Demonstration Plan, Hydrogen, Fuel Cells & Infrastructure Technologies Program, 2009.

10. A. Zuttel: Materials for hydrogen storage. *Materials Today*, Vol. 6, No. 9, 2003, pp. 24-33.

11. T.Q. Hua, R.K. Ahluwalia, J.K. Peng, M. Kromer, S. Lasher, K. McKenney, K. Law, and J. Sinha: Technical assessment of compressed hydrogen storage tank systems for automotive applications. *International Journal of Hydrogen Energy*, Vol. 36, No. 4, 2011, pp. 3037-3049.

12. A. Niedzwiecki: Storage, *Proc. Hydrogen Vision Meeting US DOE*, Washington, DC,2001.

13. Toyota Motor Sales USA Inc.: *Fuel Cell Hybrid Vehicle-Advanced*, 2010 [11/10/2010], http://www.toyota.com/esq/articles/2010/FCHV_ADV.html#.

14. I. Cumalioglu, A. Ertas, Y. Ma, and T. Maxwell: State of the art: Hydrogen storage. *Journal of Fuel Cell Science and Technology*, Vol. 5, No. 3, 2008, pp. 034001-10.

15. C. Thomas, F. Nony, S. Villalonga, and J. Renard: Research and achievements on high pressure hydrogen storage composite cylinders, *2010 SAMPE Fall Technical Conference and Exhibition, October 11, 2010 - October 14, 2010*, Salt Lake City, UT, United states,2010, pp. SAMPE's Utah Chapter.

16. J. Zhang, T.S. Fisher, P.V. Ramachandran, J.P. Gore, and I. Mudawar: A review of heat transfer issues in hydrogen storage technologies. *Journal of Heat Transfer*, Vol. 127, No. 12, 2005, pp. 1391-1399.

17. J. Zheng, X. Liu, P. Xu, P. Liu, Y. Zhao, and J. Yang: Development of high pressure gaseous hydrogen storage technologies. *International Journal of Hydrogen Energy*, Vol. 37, No. 1, 2012, pp. 1048-1057.

18. W.B. Leung, N.H. March, and H. Motz: Primitive phase diagram for hydrogen. *Physics Letters A*, Vol. 56, No. 6, 1976, pp. 425-426.

19. A. Zuttel: Hydrogen storage methods. *Naturwissenschaften*, Vol. 91, No. 4, 2004, pp. 157-172.

20. L. Schlapbach and A. Zuttel: Hydrogen-storage materials for mobile applications. *Nature*, Vol. 414, No. 6861, 2001, pp. 353-358.

21. L. Zhou: Progress and problems in hydrogen storage methods. *Renewable and Sustainable Energy Reviews*, Vol. 9, No. 4, 2005, pp. 395-408.

22. M. Pitkethly and S. Curtis: Nanomaterials and hydrogen storage. *Fuel Cell Review*, Vol. 2, No. 4, 2005, pp. 25-28.

23. L. Zhou, Y. Zhou, and Y. Sun: Enhanced storage of hydrogen at the temperature of liquid nitrogen. *International Journal of Hydrogen Energy*, Vol. 29, No. 3, 2004, pp. 319-322.

24. P. Sudan, A. Züttel, P. Mauron, C. Emmenegger, P. Wenger, and L. Schlapbach: Physisorption of hydrogen in single-walled carbon nanotubes. *Carbon*, Vol. 41, No. 12, 2003, pp. 2377-2383.

25. K.L. Lim, H. Kazemian, Z. Yaakob, and W.R.W. Daud: Solid-state materials and methods for hydrogen storage: A critical review. *Chemical Engineering & Technology*, Vol. 33, No. 2, 2010, pp. 213-226.

26. G.E. Froudakis: Hydrogen storage in nanotubes & nanostructures. *Materials Today*, Vol. 14, No. 7–8, 2011, pp. 324-328.

27. F.H.M. Spit, J.W. Drijver, W.C. Turkenburg, and S. Radelaar: Hydrogen sorption by some early-late transition metal glassesFrance,1980, pp. 8-890.

28. B. Sakintuna, F. Lamari-Darkrim, and M. Hirscher: Metal hydride materials for solid hydrogen storage: A review. *International Journal of Hydrogen Energy*, Vol. 32, No. 9, 2007, pp. 1121-1140.

29. H. Uchida and T. Kuji: Hydrogen solubility in rare earth based hydrogen storage alloys. *International Journal of Hydrogen Energy*, Vol. 24, No. 9, 1999, pp. 871-877.

30. I.P. Jain, P. Jain, and A. Jain: Novel hydrogen storage materials: A review of lightweight complex hydrides. *Journal of Alloys and Compounds*, Vol. 503, No. 2, 2010, pp. 303-339.

31. J. Yang, A. Sudik, D.J. Siegel, D. Halliday, A. Drews, R.O. Carter, C. Wolverton, G.J. Lewis, J.W.A. Sachtler, J.J. Low, S.A. Faheem, D.A. Lesch, and V. Ozolinš: A self-catalyzing hydrogen-storage material. *Angewandte Chemie International Edition*, Vol. 47, No. 5, 2008, pp. 882-887.

32. A. Zuttel, S. Rentsch, P. Fischer, P. Wenger, P. Sudan, P. Mauron, and C. Emmenegger: Hydrogen storage properties of LiBH4Annecy, France,2003, pp. 515-520.

33. L.H. Rude, T.K. Nielsen, D.B. Ravnsbæk, U. Bösenberg, M.B. Ley, B. Richter, L.M. Arnbjerg, M. Dornheim, Y. Filinchuk, F. Besenbacher, and T.R. Jensen: Tailoring properties of borohydrides for hydrogen storage: A review. *physica status solidi (a)*, Vol. 208, No. 8, 2011, pp. 1754-1773.

34. L. George and S.K. Saxena: Structural stability of metal hydrides, alanates and borohydrides of alkali and alkali- earth elements: A review. *International Journal of Hydrogen Energy*, Vol. 35, No. 11, 2010, pp. 5454-5470.

35. J. Yang and S. Hirano: Improving the Hydrogen Reaction Kinetics of Complex Hydrides. *Advanced Materials*, Vol. 21, No. 29, 2009, pp. 3023-3028.

36. K. Yvon: *Metal Hydrides: Transition Metal Hydride Complexes*, Encyclopedia of Materials: Science and Technology (Second Edition), Elsevier: Oxford, 2004, pp. 1-9.

37. P. Charvin, S. Abanades, F. Lemort, and G. Flamant: Hydrogen Production by Three-Step Solar Thermochemical Cycles Using Hydroxides and Metal Oxide Systems. *Energy & Fuels*, Vol. 21, No. 5, 2007, pp. 2919-2928.

38. A. Steinfeld: Solar thermochemical production of hydrogen–a review. *Solar Energy*, Vol. 78, No. 5, 2005, pp. 603-615.

39. A. Steinfeld: Solar hydrogen production via a two-step water-splitting thermochemical cycle based on Zn/ZnO redox reactions. *International Journal of Hydrogen Energy*, Vol. 27, No. 6, 2002, pp. 611-619.

40. A. Zuttel, A. Remhof, A. Borgschulte, and O. Friedrichs: Hydrogen: The future energy carrier. *Philosophical Transactions of the Royal Society A: Mathematical, Physical and Engineering Sciences*, Vol. 368, No. 1923, 2010, pp. 3329-3342.

41. P. Rittmeyer and U. Wietelmann: *Hydrides*, Ullmann's Encyclopedia of Industrial Chemistry, Wiley-VCH, 1996, pp. 199.

42. C.J. Smithells and C.E. Ransley: Diffusion of gases through metals. *Nature*, Vol. 134, No. 3395, 1934, pp. 814.

43. J.D. Fast: *Gases in Metals*, The MacMillan Press Ltd, Eindhoven, 1976.

44. G. Alefeld and J. Volkl: *Hydrogen in metals*, Springer-Verlag, Berlin & New York, 1978.

45. J.C. Slater: Atomic radii in crystals. *The Journal of Chemical Physics*, Vol. 41, No. 10, 1964, pp. 3199-3204.

46. W.D. Callister: *Materials Science and Engineering: An Introduction*, 7th ed, John Wiley & Sons, Inc., 2007.

47. Y. Fukai: From metal hydrides to the metal-hydrogen system. *Journal of the less-common metals*, Vol. 172, No. 1-2, 1991, pp. 8-19.

48. Y. de Ribaupierre and F.D. Manchester: Experimental study of the critical-point behaviour of the hydrogen in palladium system. I. Lattice gas aspects. *Journal of Physics C (Solid State Physics)*, Vol. 7, No. 12, 1974, pp. 2126-39.

49. J.M. Haschke and M.R. Clark: Phase equilibria and crystal growth of alkaline earth and lanthanide dihydrides. *High Temperature Science*, Vol. 7, No. 2, 1975, pp. 152-8.

50. J.A. Goedkoop and A.F. Andresen: The crystal structure of copper hydride. *Acta Crystallographica*, Vol. 8, No. 2, 1955, pp. 118-119.

51. J. Bergsma and B.O. Loopstra: The crystal structure of calcium hydride. *Acta Crystallographica*, Vol. 15, No. 1, 1962, pp. 92-93.

52. J. Ryden, B. Hjorvarsson, T. Ericsson, E. Karlsson, A. Krozer, and B. Kasemo: Unusual kinetics of hydride formation in Mg-Pd sandwiches, studied by hydrogen profiling and quartz crystal microbalance measurements. *Journal of the less-common metals*, Vol. 152, No. 2, 1989, pp. 295-309.

53. B. Vigeholm, J. Kjoller, B. Larsen, and A.S. Pedersen: Formation and decomposition of magnesium hydride, *Journal of the Less-Common Metals*, Switzerland,1983, pp. 135-44.

54. P.S. Rudman: Hydrogen-diffusion-rate-limited hydriding and dehydriding kinetics. *Journal of Applied Physics*, Vol. 50, No. 11, 1979, pp. 7195-7199.

55. J.-Y. Lee, H. Park, and J. Han: A quantitative analysis of hydriding kinetics of magnesium in a Mg/Mg₂Cu eutectic alloy. *Journal of Materials Science*, Vol. 21, No. 11, 1986, pp. 3952-3956.

56. A.S. Pedersen, K. Jensen, B. Larsen, and B. Vigeholm: Formation of hydride in pure Magnesium foils. *Journal of the less-common metals*, Vol. 131, No., 1986, pp. 31-40.

57. B. Vigeholm, K. Jensen, B. Larsen, and A.S. Pedersen: Elements of hydride formation mechanisms in nearly spherical magnesium powder particles. *Journal of the Less Common Metals*, Vol. 131, No. 1-2, 1987, pp. 133-141.

58. M. Martin, C. Gommel, C. Borkhart, and E. Fromm: Absorption and desorption kinetics of hydrogen storage alloys. *Journal of Alloys and Compounds*, Vol. 238, No. 1-2, 1996, pp. 193-201.

59. J. Huot, E. Akiba, and T. Takada: Mechanical alloying of Mg-Ni compounds under hydrogen and inert atmosphere. *Journal of Alloys and Compounds*, Vol. 231, No. 1-2, 1995, pp. 815-819.

60. M.Y. Song: Improvement in hydrogen storage characteristics of magnesium by mechanical alloying with nickel. *Journal of Materials Science*, Vol. 30, No. 5, 1995, pp. 1343-1351.

61. P.S. Rudman: Hydriding and dehydriding kinetics. *Journal of the Less Common Metals*, Vol. 89, No. 1, 1983, pp. 93-110.

62. P.E. de Jongh and P. Adelhelm: Nanosizing and Nanoconfinement: New Strategies Towards Meeting Hydrogen Storage Goals. *ChemSusChem*, Vol. 3, No. 12, 2010, pp. 1332-1348.

63. N. Cui, J.L. Luo, and K.T. Chuang: Study of hydrogen diffusion in α- and β-phase hydrides of Mg2Ni alloy by microelectrode technique. *Journal of Electroanalytical Chemistry*, Vol. 503, No. 1–2, 2001, pp. 92-98.

64. B. Kasemo and E. Tornqvist: The kinetics of hydrogen interaction with TiH_x films, $0<x<2$. *Applications of Surface Science*, Vol. 3, No. 3, 1979, pp. 307-28.

65. P.W. Atkins: *Physical chemistry*, 9th ed, W. H. Freman and Co., New York, 2010.

66. D. Moser, D.J. Bull, T. Sato, D. Noreus, D. Kyoi, T. Sakai, N. Kitamura, H. Yusa, T. Taniguchi, W.P. Kalisvaart, and P. Notten: Structure and stability of high pressure synthesized Mg-TM hydrides (TM = Ti, Zr, Hf, V, Nb and Ta) as possible new hydrogen rich hydrides for hydrogen storage. *Journal of Materials Chemistry*, Vol. 19, No. 43, 2009, pp. 8150-8161.

67. B. Baranowski: Thermodynamics of metal/hydrogen systems at high pressures. *Berichte der Bunsengesellschaft für physikalische Chemie*, Vol. 76, No. 8, 1972, pp. 714-724.

68. M. Okada, Y. Goto, R. Kataoka, Y. Yambe, A. Kamegawa, and H. Takamura: Novel hydrides in Mg-TM systems synthesized by high pressure (TM = Zr, Nb, Hf and Ta). *Journal of Alloys and Compounds*, Vol. 446-447, No., 2007, pp. 6-10.

69. C. Narayana, H. Luo, J. Orloff, and A.L. Ruoff: Solid hydrogen at 342 GPa: no evidence for an alkali metal. *Nature*, Vol. 393, No. 6680, 1998, pp. 46-49.

70. F.D. Manchester: *Phase Diagrams of Binary Hydrogen Alloys*, ASM International, Materials Park, OH, 2000.

71. B. Baranowski: Investigation of some metal-hydrogen systems in the high pressure region. *Journal of the Less Common Metals*, Vol. 101, No., 1984, pp. 115-129.

72. S. Bertil, A. Ove, and V.T. Alexandr: Phase transitions in hydrogen storage compounds under pressure. *Journal of Physics: Condensed Matter*, Vol. 19, No. 42, 2007, pp. 425201.

73. T. Takasaki, D. Kyoi, N. Kitamura, S. Tanase, and T. Sakai: Reversible hydrogen storage property and structural analysis for face-centered cubic hydride $Mg_{0.82}Zr_{0.18}H_2$ prepared by gigapascal hydrogen pressure method. *The Journal of Physical Chemistry B*, Vol. 111, No. 51, 2007, pp. 14102-14106.

74. A. Zaluska, L. Zaluski, and J.O. Strom-Olsen: Nanocrystalline magnesium for hydrogen storage. *Journal of Alloys and Compounds*, Vol. 288, No. 1-2, 1999, pp. 217-25.

75. L. Zaluski, A. Zaluska, and J.O. Strom-Olsen: Nanocrystalline metal hydrides. *Journal of Alloys and Compounds*, Vol. 253-254, No. 1-2, 1997, pp. 70-79.

76. F.H.M. Spit, J.W. Drijver, and S. Radelaar: Hydrogen sorption by the metallic glass Ni64Zr36 and by related crystalline compounds. *Scripta Metallurgica*, Vol. 14, No. 10, 1980, pp. 1071-1076.

77. C.P. Chen, B.H. Liu, Z.P. Li, J. Wu, and Q.D. Wang: The activation mechanism of Mg-based hydrogen storage alloys. *Zeitschrift fur Physikalische Chemie*, Vol. 181, No. 1-2, 1993, pp. 259-267.

78. C. Zlotea, M. Sahlberg, P. Moretto, and Y. Andersson: Hydrogen sorption properties of a Mg-Y-Ti alloy. *Journal of Alloys and Compounds*, Vol. 489, No. 2, 2010, pp. 375-378.

79. M. Sahlberg, C. Zlotea, P. Moretto, and Y. Andersson: YMgGa as a hydrogen storage compound. *Journal of Solid State Chemistry*, Vol. 182, No. 7, 2009, pp. 1833-1837.

80. T.Z. Si, Q.A. Zhang, G. Pang, D.M. Liu, and N. Liu: Structural characteristics and hydrogen storage properties of Ca3.0-xMgxNi9 (x = 0.5, 1.0, 1.5 and 2.0) alloys. *International Journal of Hydrogen Energy*, Vol. 34, No. 3, 2009, pp. 1483-1488.

81. W. Jian-Yih: Comparison of hydrogen storage properties of Ti0.37V0.38Mn0.25 alloys prepared by mechanical alloying and vacuum arc melting. *International Journal of Hydrogen Energy*, Vol. 34, No. 9, 2009, pp. 3771-3777.

82. E. Akiba, H. Hayakawa, Y. Ishido, and K. Nomura: Mg-Zn-Ni hydrogen storage alloys. *Journal of the less-common metals*, Vol. 174, No. 1-2, 1991, pp. 1071-1075.

83. K. Nomura and E. Akiba: H_2 absorbing-desorbing characterization of the Ti-V-Fe alloy system. *Journal of Alloys and Compounds*, Vol. 231, No. 1-2, 1995, pp. 513-517.

84. C. Sung-Wook, S. Gunchoo, C. Good-Sun, P. Choong-Nyeon, Y. Jeong-Hyun, and C. Jeon: Hydrogen absorption-desorption properties of $Ti0_{.32}Cr_{0.43}V_{0.25}$ alloy. *Journal of Alloys and Compounds*, Vol. 430, No. 1-2, 2007, pp. 136-141.

85. W. Luo, J. Wang, K. Stewart, M. Clift, and K. Gross: Li-Mg-N-H: Recent investigations and development. *Journal of Alloys and Compounds*, Vol. 446-447, No., 2007, pp. 336-341.

86. V. Iosub, T. Matsunaga, K. Tange, and M. Ishikiriyama: Direct synthesis of $Mg(AlH_4)_2$ and $CaAlH_5$ crystalline compounds by ball milling and their potential as hydrogen storage materials. *International Journal of Hydrogen Energy*, Vol. 34, No. 2, 2009, pp. 906-912.

87. L. Zaluski, A. Zaluska, and J.O. Strom-Olsen: Hydrogen absorption in nanocrystalline Mg2Ni formed by mechanical alloying. *Journal of Alloys and Compounds*, Vol. 217, No. 2, 1995, pp. 245-249.

88. S. Couillaud, H. Enoki, S. Amira, J.L. Bobet, E. Akiba, and J. Huot: Effect of ball milling and cold rolling on hydrogen storage properties of nanocrystalline $TiV_{1.6}Mn_{0.4}$ alloy. *Journal of Alloys and Compounds*, Vol. 484, No. 1-2, 2009, pp. 154-158.

89. N. Takeichi, K. Tanaka, H. Tanaka, T.T. Ueda, M. Tsukahara, H. Miyamura, and S. Kikuchi: Hydrogen storage properties and corresponding phase transformations

of MG/PD laminate composites prepared by a repetitive-rolling method. *Materials Transactions*, Vol. 48, No. 9, 2007, pp. 2395-2398.

90. D.R. Leiva, D. Fruchart, M. Bacia, G. Girard, N. Skryabina, A.C.S. Villela, S. Miraglia, D.S. Santos, and W.J. Botta: Mg alloy for hydrogen storage processed by SPD. *International Journal of Materials Research*, Vol. 100, No. 12, 2009, pp. 1739-1746.

91. B. Khorkounov, A. Gebert, C. Mickel, and L. Schultz: Improving the performance of hydrogen storage electrodes based on mechanically alloyed Mg61Ni30Y9. *Journal of Alloys and Compounds*, Vol. 458, No. 1-2, 2008, pp. 479-486.

92. M. Au: Hydrogen storage properties of magnesium based nanostructured composite materials. *Materials Science and Engineering B: Solid-State Materials for Advanced Technology*, Vol. 117, No. 1, 2005, pp. 37-44.

93. G. Liang, S. Boily, J. Huot, A. Van Neste, and R. Schulz: Mechanical alloying and hydrogen absorption properties of the Mg-Ni system. *Journal of Alloys and Compounds*, Vol. 267, No., 1998, pp. 302-306.

94. S. Ye, L. Ouyang, and M. Zhu: Hydrogen storage properties of preferentially orientated Mg-Ni multilayer film prepared by magnetron sputtering. *Rare Metals*, Vol. 25, No. 6, Supplement 1, 2006, pp. 295-299.

95. A. Gebert, B. Khorkounov, U. Wolff, C. Mickel, M. Uhlemann, and L. Schultz: Stability of rapidly quenched and hydrogenated Mg-Ni-Y and Mg-Cu-Y alloys in extreme alkaline medium. *Journal of Alloys and Compounds*, Vol. 419, No. 1-2, 2006, pp. 319-327.

96. S.-I. Yamaura, H.-Y. Kim, H. Kimura, A. Inoue, and Y. Arata: Thermal stabilities and discharge capacities of melt-spun Mg-Ni-based amorphous alloys. *Journal of Alloys and Compounds*, Vol. 339, No. 1-2, 2002, pp. 230-235.

97. M. Song, C.-D. Yim, S. Kwon, J.-S. Bae, and S.-H. Hong: Preparation of $Mg_{23.5}Ni_{10}$(Cu or La) hydrogen-storage alloys by melt spinning and crystallization heat treatment. *International Journal of Hydrogen Energy*, Vol. 33, No. 1, 2008, pp. 87-92.

98. D.L. Peng, M. Yan, J.F. Sun, J. Shen, Y.Y. Chen, and D.G. McCartney: Enhanced thermal stability by pre-charged hydrogen of a Zr-based bulk metallic glass. *Journal of Alloys and Compounds*, Vol. 400, No. 1-2, 2005, pp. 197-201.

99. M.V. Antisari, A. Montone, A. Aurora, M.R. Mancini, D.M. Gattia, and L. Pilloni: Scanning electron microscopy of partially de-hydrogenated MgH_2 powders. *Intermetallics*, Vol. 17, No. 8, 2009, pp. 596-602.

100. D.P. Broom: The accuracy of hydrogen sorption measurements on potential storage materials. *International Journal of Hydrogen Energy*, Vol. 32, No. 18, 2007, pp. 4871-4888.

101. D.P. Broom and P. Moretto: Accuracy in hydrogen sorption measurements. *Journal of Alloys and Compounds*, Vol. 446-447, No., 2007, pp. 687-691.

102. E. Wicke and G.H. Nernst: *Berichte Bunsengesellschaft Physikalische Chemie*, Vol. 68, No., 1964, pp. 224-235.

103. H. Züchner: Ewald Wicke and his work on metal–hydrogen systems. *Journal of Alloys and Compounds*, Vol. 330–332, No. 0, 2002, pp. 2-7.

104. T.B. Flanagan and W.A. Oates: The effect of hysteresis on the phase diagram of Pd-H. *Journal of the Less Common Metals*, Vol. 92, No. 1, 1983, pp. 131-142.

105. T. Kuji, W.A. Oates, B.S. Bowerman, and T.B. Flanagan: The partial excess thermodynamic properties of hydrogen in palladium. *Journal of Physics F: Metal Physics*, Vol. 13, No. 9, 1983, pp. 1785.

106. J. Huot, G. Liang, S. Boily, A. Van Neste, and R. Schulz: Structural study and hydrogen sorption kinetics of ball-milled magnesium hydrideSwitzerland,1999, pp. 495-500.

107. S. Qian and D.O. Northwood: Hysteresis in metal-hydrogen systems: a critical review of the experimental observations and theoretical models. *International Journal of Hydrogen Energy*, Vol. 13, No. 1, 1988, pp. 25-35.

108. J. Huot: *Metal Hydrides*, Handbook of Hydrogen Storage, Wiley-VCH Verlag GmbH & Co. KGaA, 2010, pp. 81-116.

109. H. Uchida, H. Uchida, and Y.C. Huang: Effect of the pulverization of $LaNi_5$ on the hydrogen absorption rate and the X-ray diffraction patterns. *Journal of the Less Common Metals*, Vol. 101, No., 1984, pp. 459-468.

110. M. Latroche, P.H.L. Notten, and A. Percheron-Guégan: In situ neutron diffraction study of solid gas desorption of non-stoichiometric AB_5 type hydrides. *Journal of Alloys and Compounds*, Vol. 253-254, No., 1997, pp. 295-297.

111. P.H.L. Notten, J.L.C. Daams, A.E.M. De Veirman, and A.A. Staals: In situ X-ray diffraction: a useful tool to investigate hydride formation reactions. *Journal of Alloys and Compounds*, Vol. 209, No. 1-2, 1994, pp. 85-91.

112. B. Baranowski, S. Majchrzak, and T.B. Flanagan: The volume increase of fcc metals and alloys due to interstitial hydrogen over a wide range of hydrogen contents. *Journal of Physics F: Metal Physics*, Vol. 1, No. 3, 1971, pp. 258.

113. R.K. Ahluwalia and X. Wang: Direct hydrogen fuel cell systems for hybrid vehicles. *Journal of Power Sources*, Vol. 139, No. 1–2, 2005, pp. 152-164.

114. W.H. Zachariasen, C.E. Holley, and J.F. Stamper, Jnr: Neutron diffraction study of magnesium deuteride. *Acta Crystallographica*, Vol. 16, No. 5, 1963, pp. 352-353.

115. M.U. Niemann, S.S. Srinivasan, A.R. Phani, A. Kumar, D.Y. Goswami, and E.K. Stefanakos: Nanomaterials for Hydrogen Storage Applications: A Review. *Journal of Nanomaterials*, Vol. 2008, No., 2008, pp. 9.

116. R. Schulz, J. Huot, G. Liang, S. Boily, G. Lalande, M.C. Denis, and J.P. Dodelet: Recent developments in the applications of nanocrystalline materials to hydrogen technologies. *Materials Science and Engineering A*, Vol. 267, No. 2, 1999, pp. 240-245.

117. C. Rongeat, I. Llamas-Jansa, S. Doppiu, S. Deledda, A. Borgschulte, L. Schultz, and O. Gutfleisch: Determination of the Heat of Hydride Formation/Decomposition by High-Pressure Differential Scanning Calorimetry (HP-DSC). *The Journal of Physical Chemistry B*, Vol. 111, No. 46, 2007, pp. 13301-13306.

118. S. Orimo and H. Fujii: Effects of nanometer-scale structure on hydriding properties of Mg-Ni alloys: a review. *Intermetallics*, Vol. 6, No. 3, 1998, pp. 185-92.

119. A. Zaluska, L. Zaluski, and J.O. Strom-Olsen: Synergy of hydrogen sorption in ball-milled hydrides of Mg and Mg2Ni. *Journal of Alloys and Compounds*, Vol. 289, No. 1-2, 1999, pp. 197-206.

120. H. Kan, N. Zhang, X. Wang, and H. Sun: Progress in magnesium-based hydrogen storage materials, *2nd International Conference on Civil Engineering, Architecture and Building Materials, CEABM 2012, May 25, 2012 - May 27, 2012*, Yantai, China,2012, pp. 1339-1343.

121. E. Wiberg and R. Bauer: Der magnesiumwasserstoff MgH_2. *Chemische Berichte*, Vol. 85, No. 6, 1952, pp. 593-605.

122. F.H. Ellinger, C.E. Holley, B.B. McInteer, D. Pavone, R.M. Potter, E. Staritzky, and W.H. Zachariasen: The preparation and some properties of magnesium hydride. *Journal of the American Chemical Society*, Vol. 77, No. 9, 1955, pp. 2647-2648.

123. J. Lu, Y.J. Choi, Z.Z. Fang, H.Y. Sohn, and E. RoÌˆnnebro: Hydrogen storage properties of nanosized MgH_2-0.1TiH_2 Prepared by Ultrahigh-Energy High-Pressure Milling. *Journal of the American Chemical Society*, Vol. 131, No. 43, 2009, pp. 15843-15852.

124. B. Bogdanovic, T.H. Hartwig, and B. Spliethoff: The development, testing and optimization of energy storage materials based on the MgH_2-Mg system. *International Journal of Hydrogen Energy*, Vol. 18, No. 7, 1993, pp. 575-589.

125. J.F. Stampfer, C.E. Holley, and J.F. Suttle: The magnesium-hydrogen system. *Journal of the American Chemical Society*, Vol. 82, No. 14, 1960, pp. 3504-3508.

126. M. Groll, A. Isselhorst, and M. Wierse: Metal hydride devices for environmentally clean energy technology. *International Journal of Hydrogen Energy*, Vol. 19, No. 6, 1994, pp. 507-515.

127. J. Huot, G. Liang, S. Boily, A. Van Neste, and R. Schulz: Structural study and hydrogen sorption kinetics of ball-milled magnesium hydride. *Journal of Alloys and Compounds*, Vol. 293-295, No., 1999, pp. 495-500.

128. M.-Y. Song, D.R. Mumm, S.-N. Kwon, S.-H. Hong, and J.-S. Bae: Hydrogen-storage properties of Mg-10 wt.% (Fe_2O_3, Ni, MnO) alloy prepared by reactive mechanical grinding. *Journal of Alloys and Compounds*, Vol. 416, No. 1-2, 2006, pp. 239-244.

129. H. Reule, M. Hirscher, A. Weihardt, and H. Kronmuller: Hydrogen desorption properties of mechanically alloyed MgH_2 composite materials. *Journal of Alloys and Compounds*, Vol. 305, No., 2000, pp. 246-252.

130. Z. Dehouche, J. Goyette, T.K. Bose, J. Huot, and R. Schulz: Sensitivity of Nanocrystalline MgH_2-V Hydride Composite to the Carbon Monoxide during a Long-Term Cycling. *Nano Letters*, Vol. 1, No. 4, 2001, pp. 175-178.

131. J.F.R. de Castro, S.F. Santos, A.L.M. Costa, A.R. Yavari, W.J. Botta F, and T.T. Ishikawa: Structural characterization and dehydrogenation behavior of Mg-5 at.%Nb nano-composite processed by reactive milling. *Journal of Alloys and Compounds*, Vol. 376, No. 1-2, 2004, pp. 251-256.

132. G. Barkhordarian, T. Klassen, and R.d. Bormann: Catalytic mechanism of transition-metal compounds on Mg hydrogen sorption reaction. *The Journal of Physical Chemistry B*, Vol. 110, No. 22, 2006, pp. 11020-11024.

133. N. Hanada, T. Ichikawa, and H. Fujii: Catalytic effect of nanoparticle 3d-transition metals on hydrogen storage properties in magnesium hydride MgH_2 prepared by mechanical milling. *The Journal of Physical Chemistry B*, Vol. 109, No. 15, 2005, pp. 7188-7194.

134. J. Charbonnier, P. de Rango, D. Fruchart, S. Miraglia, L. Pontonnier, S. Rivoirard, N. Skryabina, and P. Vulliet: Hydrogenation of transition element additives (Ti, V) during ball milling of magnesium hydride. *Journal of Alloys and Compounds*, Vol. 383, No. 1-2, 2004, pp. 205-208.

135. R.C. Bowman, Jr. and B. Fultz: Metallic hydrides. I. Hydrogen storage and other gas-phase applications. *MRS Bulletin*, Vol. 27, No. 9, 2002, pp. 688-693.

136. M. Paskevicius, D.A. Sheppard, and C.E. Buckley: Thermodynamic changes in mechanochemically synthesized magnesium hydride nanoparticles. *Journal of the American Chemical Society*, Vol. 132, No. 14, 2010, pp. 5077-5083.

137. W. Luo: ($LiNH_2$-MgH_2): A viable hydrogen storage system. *Journal of Alloys and Compounds*, Vol. 381, No. 1-2, 2004, pp. 284-287.

138. H.Y. Leng, T. Ichikawa, S. Hino, N. Hanada, S. Isobe, and H. Fujii: New metal-N-H system composed of $Mg(NH_2)_2$ and LiH for hydrogen storage. *The Journal of Physical Chemistry B*, Vol. 108, No. 26, 2004, pp. 8763-8765.

139. J.J. Vajo, S.L. Skeith, and F. Mertens: Reversible storage of hydrogen in destabilized $LiBH_4$. *The Journal of Physical Chemistry B*, Vol. 109, No. 9, 2005, pp. 3719-3722.

140. K. Zeng, T. Klassen, W. Oelerich, and R. Bormann: Thermodynamics of the Ni-H system. *Journal of Alloys and Compounds*, Vol. 283, No. 1-2, 1999, pp. 151-161.

141. M.L. Wayman and G.C. Weatherly: The H-Ni (Hydrogen-Nickel) system. *Bulletin of Alloy Phase Diagrams*, Vol. 10, No. 5, 1989, pp. 569-580.

142. Y. Shizuku, S. Yamamoto, and Y. Fukai: Phase diagram of the Ni-H system at high hydrogen pressures. *Journal of Alloys and Compounds*, Vol. 336, No. 1-2, 2002, pp. 159-162.

143. J.J. Reilly and R.H. Wiswall: Reaction of hydrogen with alloys of magnesium and nickel and the formation of Mg2NiH4. *Inorganic Chemistry*, Vol. 7, No. 11, 1968, pp. 2254-2256.

144. J.P. Darnaudery, M. Pezat, B. Darriet, and P. Hagenmuller: Study of allotropic transformation of Mg_2NiH_4 -Etude des transformations allotropiques de Mg_2NiH_4. *Materials Research Bulletin*, Vol. 16, No. 10, 1981, pp. 1237-1244.

145. A. Kamegawa, Y. Goto, R. Kataoka, H. Takamura, and M. Okada: High-pressure synthesis of novel compounds in an Mg-Ni system. *Renewable Energy*, Vol. 33, No. 2, 2008, pp. 221-225.

146. J. Chen, T. Sakai, N. Kitamura, H.T. Takeshita, and N. Kuriyama: High-Pressure Synthesis of Amorphous $MgNi_{1.02}H_{2.2}$. *Journal of the American Chemical Society*, Vol. 123, No. 25, 2001, pp. 6193-6194.

147. H. Kakuta, A. Kamegawa, H. Takamura, and M. Okada: Thermal stability of hydrides of magnesium-transition metal system prepared under a high pressure. *Materials Science Forum*, Vol. 350, No., 2000, pp. 329-332.

148. H. Takamura, H. Kakuta, A. Kamegawa, and M. Okada: Crystal structure of novel hydrides in a Mg - Ni - H system prepared under an ultra high pressure. *Journal of Alloys and Compounds*, Vol. 330-332, No. 0, 2002, pp. 157-161.

149. E. Rönnebro, Y. Fukai, S. Yamamoto, and T. Sakai: Phase transformations of Mg_2NiH4 at high-pressure thermal treatment. *Journal of Alloys and Compounds*, Vol. 385, No. 1-2, 2004, pp. 276-282.

150. D. Pukazhselvan, V. Kumar, and S.K. Singh: High capacity hydrogen storage: Basic aspects, new developments and milestones. *Nano Energy*, Vol. 1, No. 4, 2012, pp. 566-589.

151. H. Putz and K. Brandenburg: Pearson's Crystal Data, Crystal Structure Database for Inorganic Compounds, CD-ROM software version 1.3

152. K. Nomura, Y. Ishido, and S. Ono: Newly synthesized metal hydride $MgCaH_{3.72}$. *Yogyo-Kyokai-Shi*, Vol. 86, No. 990, 1978, pp. 67-72.

153. H. Buchner, Bernauer, and W. Strauss, *2nd Worid Hydrogen Energy Conference*, Zurich,1978, pp. 1677 - 1688.

154. Z. Gavra, M.H. Mintz, G. Kimmel, and Z. Hadari: Allotropic transitions of magnesium nickel hydride (Mg2NiH4). *Inorganic Chemistry*, Vol. 18, No. 12, 1979, pp. 3595-3597.

155. S. Ono, H. Hayakawa, A. Suzuki, K. Nomura, N. Nishimiya, and T. Tabata: Structure analysis of the metal sublattice of the low temperature form of Mg2NiH4. *Journal of the Less Common Metals*, Vol. 88, No. 1, 1982, pp. 63-71.

156. K. Nomura, E. Akiba, and S. Ono: Kinetics of the reaction between Mg_2Ni and hydrogen. *International Journal of Hydrogen Energy*, Vol. 6, No. 3, 1981, pp. 295-303.

157. B. Bogdanovic, K. Bohmhammel, B. Christ, A. Reiser, K. Schlichte, R. Vehlen, and U. Wolf: Thermodynamic investigation of the magnesium-hydrogen system. *Journal of Alloys and Compounds*, Vol. 282, No. 1-2, 1999, pp. 84-92.

158. S. Abdessameud and G.J. Rocher: Thermodynamic modeling of Mg-Ni-H coupled with key experiments, (to be submitted).

159. J.J. Reilly: Metal hydride technology. *Zeitschrift fur Physikalische Chemie. Neue Folge*, Vol. 117, No. 117, 1979, pp. 155-184.